JAMES | Journal of Advances in Modeling Earth Systems®

AGU ADVANCING EARTH AND SPACE SCIENCES

RESEARCH ARTICLE
10.1029/2023MS003916

Key Points:
- Current ecosystem models inadequately depict the lateral movement of SOC, causing uncertainties in terrestrial carbon cycle modeling
- We integrated SOC erosion and deposition into a process-based ecosystem model and evaluated it in three Chinese river basins
- Model simulations well represented observed data for the production, erosion, and deposition of organic carbon

Supporting Information:
Supporting Information may be found in the online version of this article.

Correspondence to:
W. Yuan,
yuanwpcn@126.com

Citation:
Lu, H., Wang, X., Zhang, H., Xie, X., Nakhavali, M., Quine, T. A., et al. (2024). Soil organic carbon lateral movement processes integrated into a terrestrial ecosystem model. *Journal of Advances in Modeling Earth Systems*, *16*, e2023MS003916. https://doi.org/10.1029/2023MS003916

Received 7 JUL 2023
Accepted 9 NOV 2023

Author Contributions:
Investigation: Haibo Lu
Writing – original draft: Haibo Lu
Writing – review & editing: Haibo Lu

Soil Organic Carbon Lateral Movement Processes Integrated Into a Terrestrial Ecosystem Model

Haibo Lu[1], Xiaoyuan Wang[2], Haicheng Zhang[3], Xianhong Xie[4,5], Mahdi Nakhavali[6], Timothy A. Quine[7], Wenfang Xu[8], Jiangzhou Xia[9], Bin He[10], Zhixin Hao[11], Xiu Geng[11], and Wenping Yuan[12]

[1]Department of Geography, Faculty of Arts and Sciences, Beijing Normal University, Zhuhai, China, [2]State Key Laboratory of Earth Surface Processes and Resource Ecology, Beijing Normal University, Beijing, China, [3]School of Geography and Planning, Sun Yat-sen University, Guangzhou, China, [4]State Key Laboratory of Remote Sensing Science, Jointly Sponsored by Beijing Normal University, Institute of Remote Sensing and Digital Earth of Chinese Academy of Sciences, Beijing, China, [5]Beijing Engineering Research Center for Global Land Remote Sensing Products, Faculty of Geographical Science, Institute of Remote Sensing Science and Engineering, Beijing Normal University, Beijing, China, [6]International Institute for Applied Systems Analysis, Laxenburg, Austria, [7]Department of Geography, College of Life and Environmental Sciences, University of Exeter, Exeter, UK, [8]Key Laboratory of Vegetation Restoration and Management of Degraded Ecosystems, South China Botanical Garden, Chinese Academy of Sciences, Guangzhou, China, [9]Tianjin Key Laboratory of Water Resources and Environment, Tianjin Normal University, Tianjin, China, [10]College of Global Change and Earth System Science, Beijing Normal University, Beijing, China, [11]Key Laboratory of Land Surface Pattern and Simulation, Institute of Geographic Sciences and Natural Resources Research, Chinese Academy of Sciences, Beijing, China, [12]College of Urban and Environmental Sciences, Institute of Carbon Neutrality, Sino-French Institute for Earth System Science, Peking University, Beijing, China

Abstract Lateral movement of soil organic carbon (SOC) induced by soil erosion and runoff changes spatial distributions of SOC, and further changes the land-atmosphere CO_2 exchange and terrestrial carbon budget. However, current ecosystem models do not or only poorly integrate the process of SOC lateral movement and cannot simulate the impacts of soil erosion on the carbon cycle. This study integrated SOC erosion and deposition processes into a process-based ecosystem model (i.e., Integrated BIosphere Simulator (IBIS)), and separately simulated the lateral movements of dissolved organic carbon (DOC) and particulate organic carbon (POC). The model was evaluated in three river basins in Northeast China that are dominated by cropland, forest, and grassland. The results showed that the model reproduced well the production, erosion, and deposition of DOC and POC. The annual SOC lateral movement (1.34–7.22 g C m^{-2} yr^{-1}) induced by erosion in the three tested basins was 0.27%–1.45% of the annual net primary production. The model developed in this study has great implications for simulating the lateral movements of SOC in terrestrial ecosystems, which can improve model performance in projecting the terrestrial carbon budget.

Plain Language Summary Lateral movement of soil organic carbon (SOC) with soil erosion and runoff is an important process in estimating land carbon budget. However, the current ecosystem models are not or poorly integrated this process, and cannot simulate the impacts of lateral movement of SOC on carbon cycle. This study integrates SOC erosion and deposition processes into a process-based ecosystem model (Integrated BIosphere Simulator (IBIS)), and separately simulates the lateral movements of dissolved organic carbon (DOC) and particulate organic carbon (POC). The model was evaluated at three river basins in Northeast China dominated by cropland, forest and grassland, respectively. The results showed the model can reproduce well the production, erosion, deposition of DOC and POC. The model developed in this study has great implications for simulating the lateral movements of SOC in terrestrial ecosystem, which can improve model performance on projecting terrestrial carbon budget.

1. Introduction

The terrestrial ecosystem plays an important role in regulating the atmospheric concentration of carbon dioxide (CO_2) (Yuan et al., 2018). However, estimates of the terrestrial carbon cycle remain largely uncertain because some important ecosystem processes are still missing in current ecosystem models (IPCC, 2014). The lateral movement of soil organic carbon (SOC) over the land surface, induced by soil erosion and runoff, is either ignored or inadequately represented in current terrestrial ecosystem models, and potentially results in uncertainties in our estimations of the terrestrial carbon budget (Quinton et al., 2010; Tan et al., 2022; Yue et al., 2016; Zhang et al., 2014). Previous studies reported 75–201 Pg of global soil erosion annually, which caused 1.6–6 Pg C of SOC redistribution each year (Ito, 2007; Lal, 2003; Yang et al., 2003). The lateral movement of SOC substantially impacts the terrestrial ecosystem carbon budget by regulating several key ecosystem processes. First, soil erosion accelerates SOC erosion of the surface soil and reduces the available SOC for decomposition at eroded sites, resulting in the deep burial of SOC and the simultaneous inhibition of decomposition at deposition locations (Lal, 2004; Yoo et al., 2005). Second, during the detachment and transport processes, the chemical or physical breakdown of soil aggregates may increase SOC decomposition, especially for dissolved organic carbon (DOC) (Kalbitz et al., 2000). Third, there is a large volume of SOC in river system, which have a higher decomposition rate than that in the land (Cole et al., 2007). Therefore, it is necessary to integrate the lateral movement of SOC into terrestrial ecosystem models (Zhang et al., 2014).

Several studies have focused on integrating soil carbon lateral movements into ecosystem models by incorporating empirical and process-based hydrology models into ecosystem models (Batson et al., 2015; Dick et al., 2015; Futter et al., 2007; Lauerwald et al., 2017; Liao et al., 2019; Lu & Zhuang, 2015; Nakhavali et al., 2020; Ren et al., 2016; Skjemstad et al., 2004). The performance of these models depends highly on the capability of integrated hydrology models. One of the most important limitations is that the integrated hydrology models neglect the deposition and transportation of the eroded soil, which induces a vital carbon sink (Berhe et al., 2007). A recent study, based on two national survey data sets in China during 1995–1996 and 2010–2012, found that on average 47%–57% of the eroded SOC was deposited over land in the nine river basins of China (Wang et al., 2019). Increasing evidence has highlighted that the deposition of SOC over land is one of the most important processes for quantifying the impacts of SOC erosion on the carbon cycle because of the strong protection of SOC at the deposition sites (Davidson & Janssens, 2006). For example, the SOC mineralization rate in deposition sites was only one-third of that in slope lands because the high soil moisture and compaction in deposition sites can constrain carbon mineralization by limiting the oxygen availability to SOC decomposition (Zhang et al., 2016).

In addition, several important processes regulating the lateral movements of DOC are still missing in most models. Numerous studies have highlighted that the transfer of DOC from terrestrial ecosystems to aquatic ecosystems highly impacts the land-atmosphere carbon exchange (Battin et al., 2009; Casas-Ruiz et al., 2023; Lauerwald et al., 2017). Although several experiments have revealed the important processes of DOC production (Harrison et al., 2008; Liebmann et al., 2020; Neff & Asner, 2001), they have not been quantitatively represented in terrestrial ecosystem models. First, root exudation is an important source of DOC (Jones & Donnelly, 2004; van Hees et al., 2005). For example, a previous study found a 45% reduction in DOC after the girdling of a tree stand (Högberg & Högberg, 2002), a treatment which stops the flux of photosynthate from the tree canopy to the roots and their associated microorganisms. However, this process is poorly integrated into models for simulating DOC production in soil. Second, throughfall and stemflow, enriched in tree-DOC relative to rainfall, are only integrated in a few models for simulating soil DOC production (Lauerwald et al., 2017). Rainwater interacts with trees picking up DOC within the canopy, which is then exported from the tree in stemflow and throughfall. The DOC concentrations of stemflow (5–200 mg C L^{-1}) (Levia et al., 2011; Moore, 2003; Tobón et al., 2004) and throughfall (1–100 mg C L^{-1}) (Inamdar et al., 2012; Le Mellec et al., 2010; Michalzik et al., 2001; Neff & Asner, 2001) are much larger than those of rainwater (0.3–2 mg C L^{-1}) (Willey et al., 2000). Carbon compounds coming from throughfall are easily decomposable for decomposition and mineralization; hence, they increase the leaching of DOC from the forest floor (Michalzik et al., 2001). A previous study also showed that the annual DOC flux in the forest floor was positively correlated with the throughfall DOC flux (Michalzik et al., 2001). Additionally, runoff over the land surface strongly determines the magnitude of lateral DOC movements and affects the POC associated with sediment loads. Especially for POC, surface runoff and soil erosion are the primary control on the lateral movement of biogenic POC from the terrestrial ecosystems to aquatic environments (Galy et al., 2015). The global flux of terrestrial POC to the ocean is approximately 160 Mt C yr^{-1} (Galy et al., 2015). Climate change (e.g., intensified rainfall) can increase the terrestrial POC exports to river networks via enhanced runoff and soil erosion (Hilton et al., 2012). Land cover and land use change substantially impact the magnitude of soil and SOC erosion (Chaplot et al., 2005). Several studies have reported a larger sensitivity of surface runoff and erosion to land cover than to climate change (Khoi & Suetsugi, 2014; Simonneaux et al., 2015). Previous studies reported that the conversion of natural forests to agricultural land can facilitate the POC transfer to fluvial system due to the increased soil erosion rates (Guillaume et al., 2015; Jeong et al., 2012).

10.1029/2023MS003916

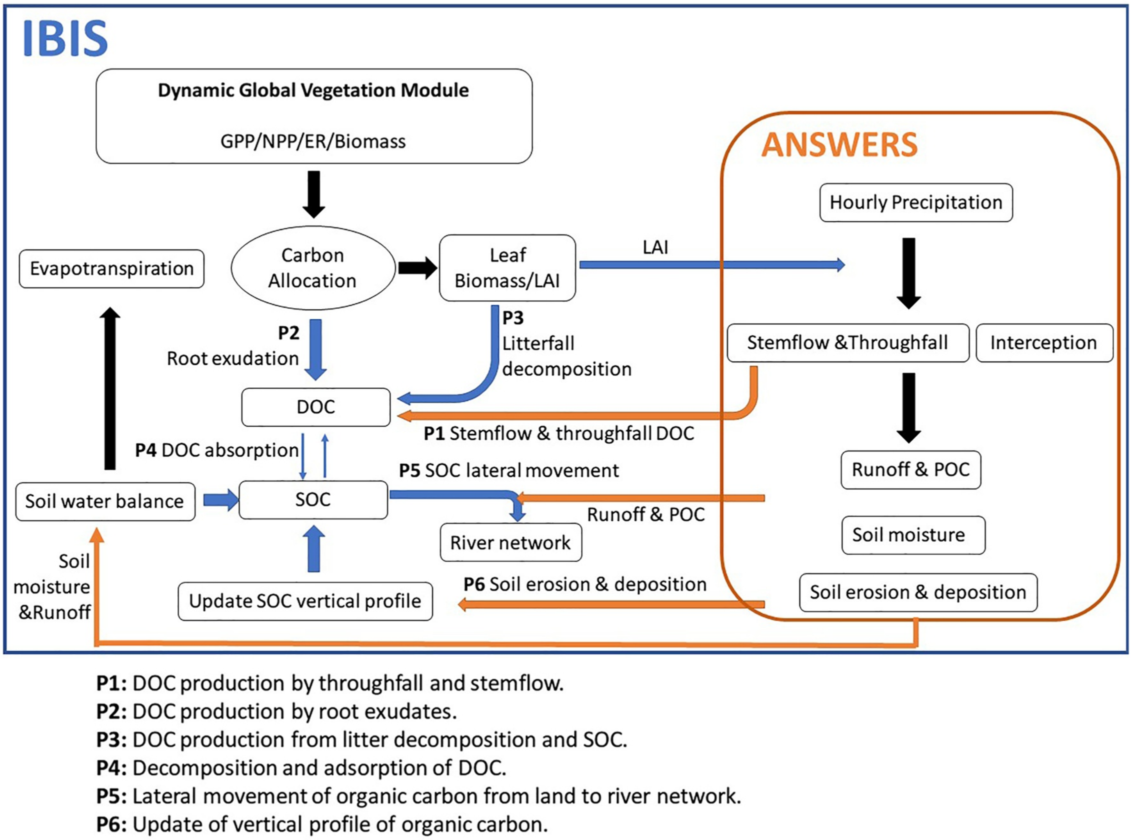

Figure 1. Schematic diagram of the interaction between the IBIS and ANSWERS model. P1 to P6 indicate the new soil carbon processes developed in this study. GPP, NPP and ER indicate Gross Primary Production, Net Primary Production and Ecosystem Respiration, respectively.

In this study, we developed a new process-based soil erosion model that can depict the erosion and deposition of SOC induced by soil erosion, as well as the production and decomposition of DOC and POC associated with root exudation, throughfall, stemflow and ground runoff. We integrated this soil erosion model into a terrestrial ecosystem model (Integrated BIosphere Simulator (IBIS); Kucharik et al., 2000; Yuan et al., 2014) to quantify the lateral movement of SOC induced by soil erosion. We validated the performance of the upgraded terrestrial ecosystem model against the observations of river runoff, sediment load and riverine POC and DOC from three river basins dominated by different vegetation types in Northeast China. Then, we simulated SOC erosion and deposition over three river basins using the newly developed model and analyzed the differences in lateral movements of SOC among them.

2. Model Description

In this study, we developed a new process-based erosion model to quantify the lateral movements of SOC over the land surface, which includes the production, erosion, transport, and deposition processes of two organic carbon components, POC and DOC. This study integrated the lateral movements of SOC into the IBIS model. IBIS is a comprehensive terrestrial ecosystem model. It simulates the change and balance of water, energy and carbon, which show the vertical carbon fluxes in biophysical, physiological and ecological processes (Kucharik et al., 2000; Liu et al., 2014; Song et al., 2020; Yuan et al., 2014). In IBIS, we fully coupled a hydrological model (i.e., Areal Nonpoint Source Watershed Environment Response Simulation (ANSWERS)) that explicitly represented surface runoff, sediment load, and the production and transfer of two organic carbon components (DOC and POC) (Figure 1). This study did not integrate the impacts of subsurface runoff process on DOC and POC due to its small contributions (Tiefenbacher et al., 2021).

The ANSWERS model includes rainfall, interception, infiltration, surface detention, surface retention, runoff and subsurface drainage (Silburn & Connolly, 1995). Following hydrologic processes, soil erosion and deposition in ANSWERS are separated into detachment and transport processes. The detachment algorithms of raindrop and overland flow (Meyer & Wischmeier, 1969) are used with empirical soil erosivity, cropping and management factors from the Universal Soil Loss Equation (USLE) (Wischmeier & Smith, 1978). The detachment equations used in this study were developed based on physical processes from the Water Erosion Prediction Project (WEPP) (Alberts et al., 1995). The original ANSWERS used a four-direction flow method to simulate water and sediment travel from a given cell to adjacent cells. There are eight valid output directions relating to the eight adjacent cells into which the flow could travel. Therefore, we used an eight-direction flow model and followed an approach presented by Jenson and Domingue (1988) to improve the original simulations in ANSWERS.

In this integrated model, the influence of the change in (or additional) SOC pool mainly includes four aspects (Figure S1). First, we added the production and decomposition of DOC pool in IBIS, on the basis of the original carbon pools. Second, the lateral movement of SOC pool is induced by soil erosion and deposition simulated in ANSWERS. Third, after erosion and deposition of SOC in the topsoil, we updated the vertical evolution of SOC pool in each layer of IBIS. Fourth, the DOC and POC from land to rivers is estimated based on runoff and sediment loads simulated by ANSWERS and DOC pool in IBIS.

The three major processes for simulating the lateral carbon movements from land to rivers are (a) the production and decomposition of organic carbon (DOC and POC) in the land, (b) the lateral movement of organic carbon from land to river network, and (c) updating the vertical profile of organic carbon. In the following sections we briefly describe the key algorithms used to simulate these four processes.

2.1. Production and Decomposition of Organic Carbon in Soil

The formation and decomposition of SOC have been well represented in the default IBIS (Kucharik et al., 2000; Liu et al., 2014), and this study mainly developed the processes of DOC production and decomposition. The dynamics of DOC is one of the most important processes related to the lateral carbon movement. Following the water path through a forest ecosystem, there are numerous sources and sinks of DOC. Precipitation incorporates atmospheric aerosol ingredients, such as dust and gases, which contain organic carbon. Rainwater moves through the atmosphere, washes through the forest canopy, infiltrates and percolates the forest litter layer and the organic-matter-rich topsoil, and then passes downward through the deeper mineral soil, reaching groundwater tables and entering the aquifer. Important sources of DOC, especially in the surface soil layers, are decomposition products of root exudates (Baetz & Martinoia, 2014; Tückmantel et al., 2017), plant litter (Bantle et al., 2014; Klotzbücher et al., 2013; Magnússon et al., 2016) and SOC (Hagedorn et al., 2004; Kalbitz et al., 2007; Mueller et al., 2009).

In general, DOC can be grouped into labile and recalcitrant DOC (Marschner & Kalbitz, 2003). Labile DOC consists mainly of simple carbohydrate compounds (i.e., glucose and fructose), low molecular weight (LMW) organic acids, amino sugars, and LMW proteins (Kaiser et al., 2001). Recalcitrant DOC consists of polysaccharides (i.e., the breakdown products of cellulose and hemicellulose) and other plant compounds, and/or microbially derived degradation products (Marschner & Kalbitz, 2003). The chemical composition of DOC, in turn, depends on the DOC source and its processing along the water flow path through ecosystems (Bolan et al., 2011).

2.1.1. DOC Production by Throughfall and Stemflow

Throughfall is the water that drips through the leaves of the canopy, while stemflow denotes water flowing down the tree trunk. Organic compounds are released from leaves (Wickland et al., 2007), twigs and tree stems (Levia & Germer, 2015), insects (Michalzik et al., 2016), and bacteria inhabiting the canopy and leaf surfaces (Lindow & Brandl, 2003). Both throughfall and stemflow were enriched in DOC compared to rainwater (Inamdar et al., 2012; Levia et al., 2011).

The DOC production via throughfall (DOC_{thr}, g C m^{-2}) was calculated as follows:

$$DOC_{thr} = EN_{thr} \times \left(DOC_{prec} \times R_{thr}\right) \tag{1}$$

where EN_{thr} is the enrichment ratio, DOC_{prec} is the DOC concentration in the rainwater (g C mm^{-1} m^{-2}), and R_{thr} (mm) is the simulated throughfall by IBIS. In this study, we set DOC_{prec} to 0.003 g C mm^{-1} m^{-2} according to the mean values of measurements in Asia (Iavorivska et al., 2016).

A recent study showed a distinct seasonality of the enrichment ratio of throughfall, and the enrichment ratio in summer was significantly higher than those of other seasons (You et al., 2020). The reason for such seasonality may be that the deposited dissolved organic matter is higher due to the larger leaf area in summer. We used the following equation to calculate the enrichment ratio of throughfall:

$$\mathrm{EN_{thr}} = E_{\mathrm{bra}} + E_{\mathrm{leaf}} \times \frac{\mathrm{LAI} - \mathrm{LAI_{min}}}{\mathrm{LAI_{max}} - \mathrm{LAI_{min}}} \quad (2)$$

where E_{bra} and E_{leaf} indicate the basic enrichment ratios contributed by branches and leaves, respectively, which were equal to 1.2 and 1.5 respectively. The LAI is the leaf area index (m^2 · m^{-2}) simulated by IBIS. The LAI_{min} and LAI_{max} indicate the minimum and maximum LAI during the growing season, respectively. The second item on the right side of Equation 2 shows the enrichment ratio contributed by plant leaves, which varies with leaf growth during the growing season.

The DOC production via stemflow (DOC_{ste}, g C m^{-2}) was calculated using the Levia and Herwitz (2000) method as follows:

$$\mathrm{DOC_{ste}} = \mathrm{EN_{ste}} \times \left(\mathrm{DOC_{prec}} \times \mathrm{Rain}\right) \times B_a \quad (3)$$

where EN_{ste} indicates the stemflow enrichment ratio per unit trunk basal area (m^{-2}), and B_a is the truck basal area (m^2) simulated by IBIS. The streamflow enrichment ratio was profoundly affected by tree size, where small trees had a higher flux-based DOC enrichment ratio and produced more DOC per unit trunk basal area (Chen et al., 2019). The linear degression equation was used to simulate the streamflow enrichment ratio according to Chen et al. (2019) as follows:

$$\mathrm{EN_{ste}} = -1.11 \times \mathrm{DBH} + 111.65 \quad (4)$$

where DBH is the diameter at breast height (cm) simulated by IBIS.

2.1.2. DOC Production From Litter Decomposition and SOC

The IBIS model includes a fully coupled soil biogeochemistry module (Kucharik et al., 2000), which separates the plant litter and SOC into three pools according to the decomposition rates. In this study, we integrated a DOC pool into the IBIS model (Figure 1). The DOC production from litterfall (DOC_{lit}, g C m^{-2} day^{-1}) and microbial (DOC_{mic}, g C m^{-2} day^{-1}) and soil organic carbon (DOC_{soc}, g C m^{-2} day^{-1}) were calculated as follows:

$$\mathrm{DOC}_{\mathrm{lit},i} = \mathrm{Slit}_k \times R_{k,i} \times T_s \times W_s \quad (5)$$

$$\mathrm{DOC}_{\mathrm{mic},i} = \mathrm{Smic} \times R_{k,i} \times T_s \times W_s \quad (6)$$

$$\mathrm{DOC}_{\mathrm{soc},i} = \mathrm{Ssoc}_k \times R_{k,i} \times T_s \times W_s \quad (7)$$

$$T_s = Q_{10}^{\frac{T-T_0}{10}} \quad (8)$$

$$W_s = \begin{cases} e^{\frac{(\mathrm{wfps}-60)\times(\mathrm{wfps}-60)}{-800}}, wfps<60 \\ 0.00037 \times \mathrm{wfps}^2 - (0.0748 \times \mathrm{wfps}) + 4.13, \mathrm{wfps} \geq 60 \end{cases} \quad (9)$$

where $DOC_{lit,i}$, $DOC_{mic,i}$, and $DOC_{soc,i}$ represent the production rate of the ith DOC component ($i = 1$ for the liable pool; $i = 2$ for the recalcitrant pool; Figure 1) (g C m^{-2} day^{-1}); $Slit_k$, $Smic_k$ and $Ssoc_k$ indicate organic carbon pools of litterfall (c1: $k = 1$; c2: $k = 2$), microbes (c4: $k = 4$), and soil (c8: $k = 8$; c9: $k = 9$; c10: $k = 10$) (Figure 1); $R_{k,i}$ indicates the maximum DOC production rate (g C m^{-2} day^{-1}) from the kth litterfall and microbial and soil organic carbon pool to the ith DOC pool; T_s and W_s represent the restriction functions of the soil temperature and soil moisture, which are assumed to be same for all DOC pools; T and wfps represent the soil temperature and water-filled pore space percentage, respectively; and Q_{10} and T_0 are two parameters of the Q_{10} temperature function, and are set to 2°C and 0°C, respectively. For aboveground litterfall, the soil temperature and moisture of the first soil layer were used, and the mean soil temperature and moisture of the top soil layer (0–30 cm) simulated by IBIS were used for the belowground litterfall and microbial and soil organic carbon. In this study, soil organic carbon pools were discretized through the profiles of soil layers (Section 2.3) and simulated the soil organic pools in each soil layer.

2.1.3. DOC Production by Root Exudates

The DOC production from root exudates at the jth soil layer ($DOC_{ex,j}$) was simulated as the follows:

$$\mathrm{DOC}_{\mathrm{ex},j} = \mathrm{NPP} \times \mathrm{CA}_{\mathrm{root}} \times \mathrm{RE} \times R_j \times \mathrm{Coef} \tag{10}$$

where NPP is the net primary production simulated by IBIS (g C m^{-2} day^{-1}), CA_{root} is the carbon allocation ratio of photosynthates to fine roots (%), RE indicates the percentage of root exudates accounting for the NPP of the fine roots [and is set to 40% according to Lynch and Whipps (1990)], R_j is the ratio of fine roots in jth soil layer (%), and Coef is the DOC production coefficient from the root exudates (g C g^{-1} root exudates; 55%) (Högberg & Högberg, 2002). The allocation ratio of the photosynthate to fine roots in IBIS was simulated based on a resource availability model (Xia et al., 2014), and the carbon allocation was determined by soil water, nitrogen, and light availability. In addition, the IBIS model integrates a dynamic root growth model (Lu et al., 2019), which represents the vertical distribution ratio of the fine roots (i.e., R_j) over the soil layers.

By incorporating all the above sources, the production rate of liable DOC (DOC_{lab}) and recalcitrant DOC (DOC_{rec}) is simulated as follows:

$$\mathrm{DOC}_{\mathrm{lab}} = \alpha_{\mathrm{thr}} \times \mathrm{DOC}_{\mathrm{thr}} + \alpha_{\mathrm{ste}} \times \mathrm{DOC}_{\mathrm{ste}} + \alpha_{\mathrm{ex}} \times \mathrm{DOC}_{\mathrm{ex}} + \mathrm{DOC}_{\mathrm{lit},1} + \mathrm{DOC}_{\mathrm{mic},1} + \mathrm{DOC}_{\mathrm{soc},1} \tag{11}$$

$$\begin{aligned}\mathrm{DOC}_{\mathrm{rec}} = {} & (1-\alpha_{\mathrm{thr}}) \times \mathrm{DOC}_{\mathrm{thr}} + (1-\alpha_{\mathrm{ste}}) \times \mathrm{DOC}_{\mathrm{ste}} + (1-\alpha_{\mathrm{ex}}) \\ & \times \mathrm{DOC}_{\mathrm{ex}} + \mathrm{DOC}_{\mathrm{lit},2} + \mathrm{DOC}_{\mathrm{mic},2} + \mathrm{DCO}_{\mathrm{soc},2}\end{aligned} \tag{12}$$

where α_{thr}, α_{ste} and α_{ex} indicate the percentage of labile DOC accounting for total DOC sources from throughfall, stemflow, and root exudates, respectively. The production rates of labile and recalcitrant DOC from litterfall and microbial and soil organic carbon decomposition were directly simulated according to Equations 5–7 (1 for labile pool; 2 for recalcitrant pool). A recent incubation-based experiment showed that the DOC from throughfall and stemflow had the higher decomposition rates than from litter leachate (Thieme et al., 2019) because they included a higher percentage of labile DOC components (Kalbitz et al., 2000). Therefore, we set the higher partition ratio of DOC to labile DOC from throughfall ($\alpha_{thr} = 0.8$) and stemflow ($\alpha_{ste} = 0.8$), and set α_{ex} as 0.5.

2.1.4. Decomposition and Adsorption of DOC

The decomposition of DOC pools (D_{DOC}; g C m^{-2} day^{-1}) follows first-order kinetics depending on the temperature and DOC pool size as follows

$$D_{\mathrm{DOC},i} = S_{\mathrm{DOC},i} \times \left(1 - e^{(-K_{\mathrm{DOC},i} \times T_s)}\right) \tag{13}$$

where $S_{DOC,\,i}$ is the pool size (g C m^{-2}) of labile ($i = 1$) and recalcitrant ($i = 2$) DOC; $K_{DOC,\,i}$ is the basal decomposition rate of the liable and recalcitrant DOC (day^{-1}; $K_{DOC,1} = 0.3$; $K_{DOC,2} = 0.0016$; Nakhavali et al., 2018); T_s is the regulation scale of temperature on the decomposition of DOC, and we assumed the same temperature regulations for both labile and recalcitrant DOC, which were calculated using in Equation 8. Except for the decomposed DOC that was partly respired into the atmosphere (R_{DOC} in g C m^{-2} day^{-1}), the remaining decomposed DOC returned to the microbial carbon pool (Smic in g C m^{-2} day^{-1}, Figure 1). We used a fixed carbon use efficiency (CUE) (i.e., 0.5; Manzoni et al., 2012) to represent the partitioning of DOC between respiration and microbial biomass (Kalbitz et al., 2003; Nakhavali et al., 2018).

$$\mathrm{Smic} = \mathrm{Smic} + \mathrm{CUE} \times D_{\mathrm{DOC},i} \tag{14}$$

$$R_{\mathrm{DOC},i} = (1 - \mathrm{CUE}) \times D_{\mathrm{DOC},i} \tag{15}$$

Moreover, we also estimated the sorption of DOC which is one of the key processes related to DOC concentrations in soil solutions (Moore et al., 2008). In this study, a constant sorption coefficient (K_D) was used to simulate the adsorbed DOC ($\mathrm{ADP}_{\mathrm{DOC},i}$), followed by Nakhavali et al. (2018).

$$\mathrm{ADP}_{\mathrm{DOC},i} = S_{\mathrm{DOC},i} \times K_D \times \frac{\mathrm{BK}}{\theta} \tag{16}$$

where $S_{\mathrm{DOC},i}$ is the dissolved labile and recalcitrant DOC pools, K_D is the distribution factor (8.05×10^{-6} m^3 water kg^{-1} soil; Nakhavali et al., 2018), BK is the bulk density (kg soil m^{-3}), the θ is the volumetric soil moisture (m$^3 \cdot$ m^{-3}) simulated by the ANSWERS model.

2.2. Lateral Movement of Organic Carbon From Land to River Network

The magnitude of DOC movement from soil to rivers can be simulated with the following equation:

$$L_{\mathrm{DOC},i} = \mathrm{RO} \times \frac{S_{\mathrm{DOC},i}}{S_{\mathrm{H2O}}} \tag{17}$$

where $L_{\mathrm{DOC},\,i}$ is the DOC flux from the soil to the river system (g C s^{-1}), RO is the simulated runoff of the land surface (mm s^{-1}) by the ANSWERS model, $S_{\mathrm{DOC},\,i}$ is the pool size (g C m^{-2}) of the labile ($i = 1$) and recalcitrant ($i = 2$) DOC in the top soil layer (0–5 cm, see Section 2.3), and S_{H2O} is the water contained in the top soil layer (mm).

The POC exported from the soil to rivers is assumed to occur with sediment loading (R_{soil}, g m^{-2} d^{-1}), which was simulated by ANSWERS. In this study, we used a simplified method to simulate the erosion rates of POC (R_{poc}, g C m^{-2} d^{-1}) with sediment in the soil and rivers. We used a fixed POC concentration to SOC in the soil column ($\mathrm{POC}_{\mathrm{con}}$, g C g soil^{-1}).

$$R_{\mathrm{poc}} = \mathrm{POC}_{\mathrm{CON}} \times R_{\mathrm{soil}} \tag{18}$$

It should be noticed that the lateral movement of organic carbon from land to river may not be a strictly lateral transport in this study. Because a land grid cell may not be a neighbor of a river cell, from which the runoff cannot directly flow into the river. In that case, the lateral transport is a teleport. In this study, we assumed that this teleport is also included in the land-river lateral movement of organic carbon.

2.3. Update of Vertical Profile of Organic Carbon

Soil erosion and deposition substantially changed the vertical distribution of SOC. Erosion transports fresh organic matter that is present at or near the soil surface. A significant portion of the eroded, C-rich topsoil is buried in different depositional settings, rather than flowing into rivers. After successive erosion events, the C-rich topsoil of the eroding slopes is buried in the depositional lowlands and becomes a subsoil horizon of the convergent slopes or plains (Berhe et al., 2007). The soil was discretized into 10 layers in the IBIS model (i.e., 0–5 cm, 5–10 cm, 10–15 cm, 15–20 cm, 20–30 cm, 30–50 cm, 50–80 cm, 80–120 cm, 120–200 cm, 200–400 cm), and the SOC decreased with soil depth represented by the following equations:

$$\mathrm{CSOC}_i = 1 - \beta^d \tag{19}$$

$$\mathrm{SOC}_i = (\mathrm{CSOC}_i - \mathrm{CSOC}_{i-1}) \times \mathrm{SOC} \tag{20}$$

where CSOC_i is the cumulative SOC proportion (between 0 and 1) from the soil surface to the ith soil layer, d is depth from the soil surface to the ith layer (cm), β is the extinction coefficient, SOC_i is the soil organic carbon concentration of the ith layer, and SOC is the entire soil organic pool.

Our model used the method developed by Zhang et al. (2020) to represent the vertical evolution of SOC resulted from soil erosion and deposition in the IBIS model. The daily SOC delivery rate (DRC_j, g C m^{-2} day^{-1}) in pixel j

to the adjacent downstream pixel k induced by soil erosion is calculated based on the average SOC concentration in the top three soil layers (0–15 cm), shown as:

$$Z_j = \frac{\mathrm{ER}_j}{\mathrm{BD}_j} \tag{21}$$

$$\mathrm{SOCT}_j = \sum\nolimits_i^3 \mathrm{SOC}_{ij} \tag{22}$$

$$\mathrm{DRC}_j = \frac{Z_j}{H_i}\mathrm{SOCT}_j \tag{23}$$

where Z_j is the thickness of eroded soil in pixel j (m day^{-1}), ER_j is the amount of soil erosion in pixel j (g m^{-2} day^{-1}), BD_j is the soil bulk density in pixel j (g m^{-3}), SOCT_j is the sum of SOC stock in the top three soil layers in pixel j (g C m^{-2}), SOC_{ij} is the SOC stock of the ith soil layer in pixel j (g C m^{-2}), H_i is the depth at the bottom of the ith soil layer (m), here i is equal to 3.

The amount of eroded SOC from the pixel j or SOC deposition to the next pixel k in the top three soil layers is proportional to the original SOC stock in the corresponding soil layer. The SOC stock in fourth to 10th layers at eroded pixel j is transported from deep layer to surface layer, and at deposited pixel k is transported in the opposite direction. Therefore, original SOC in deeper soil layers will be exposed at eroded site, and in surface soil layers will be stored at deposited site. The updated SOC stock of the ith soil layer at eroded pixel j and deposited pixel k ($\mathrm{SOC}_{\mathrm{ij\_new}}$ and $\mathrm{SOC}_{\mathrm{ik\_new}}$, g C m^{-2}, respectively) is calculated along with vertical soil layer:

$$\mathrm{SOC}_{\mathrm{ij\_new}} = \begin{cases} \left(\left(1-\frac{Z_j}{H_3}\right)\mathrm{SOCT}_j + \frac{Z_j}{H_4-H_3}\mathrm{SOC}_{4j}\right)\frac{\mathrm{SOC_{ij}}}{\mathrm{SOCT}_j}, & i \le 3 \\ \left(1-\frac{Z_j}{H_i-H_{i-1}}\right)\mathrm{SOC_{ij}} + \frac{Z_j}{H_{i+1}-H_i}\mathrm{SOC}_{(i+1)j}, & 4 \le i \le 9 \\ \left(1-\frac{Z_j}{H_i-H_{i-1}}\right)\mathrm{SOC_{ij}}, & i = 10. \end{cases} \tag{24}$$

$$\mathrm{SOC}_{\mathrm{ik\_new}} = \begin{cases} \left(\frac{Z_j}{H_3}\mathrm{SOCT}_j + \left(1-\frac{Z_j}{H_3}\right)\mathrm{SOCT}_k\right)\frac{\mathrm{SOC_{ik}}}{\mathrm{SOCT}_k}, & i \le 3 \\ \frac{Z_j}{H_3}\mathrm{SOCT}_k + \left(1-\frac{Z_j}{H_i-H_{i-1}}\right)\mathrm{SOC_{ik}}, & i = 4 \\ \frac{Z_j}{H_{i-1}-H_{i-2}}\mathrm{SOC}_{(i-1)k} + \left(1-\frac{Z_j}{H_i-H_{i-1}}\right)\mathrm{SOC_{ik}}, & 5 \le i \le 9 \\ \frac{Z_j}{H_{i-1}-H_{i-2}}\mathrm{SOC}_{(i-1)k} + \mathrm{SOC_{ik}}, & i = 10. \end{cases} \tag{25}$$

where SOCT_k is the sum of SOC stock in the top three soil layers in pixel k (g C m^{-2}), SOC_{ik} is the SOC stock of the ith soil layer in pixel k (g C m^{-2}).

3. Study Area, Data, and Model Operation

3.1. Study Area

We selected three sub-basins in the upstream regions of the Songhua River Basin in the Northeast China, which is without water reservoirs and dams to avoid anthropogenic perturbations (Figure 2a). In addition, these three sub-basins are dominated by forest, grassland, and cropland, respectively (Figures 2e–2g; Table 1), and the model performance can be evaluated for the various vegetation types. The study area is characterized by a temperate continental monsoon climate, with an average annual temperature of 3–5°C and annual precipitation of 500 mm. Precipitation from June to September accounts for 60%–80% of the annual precipitation. We collected the measurements of runoff and sediment loads of the three sub-basins from to 2008–2016 at the hydrology stations of Chenming (46°58′ N, 29°29′ E), Kumotun (49°26′ N, 125°15′ E), and Wudaogou (42°53′ N, 126°38′ E). Detailed information on three sub-basins is provided in Table 1.

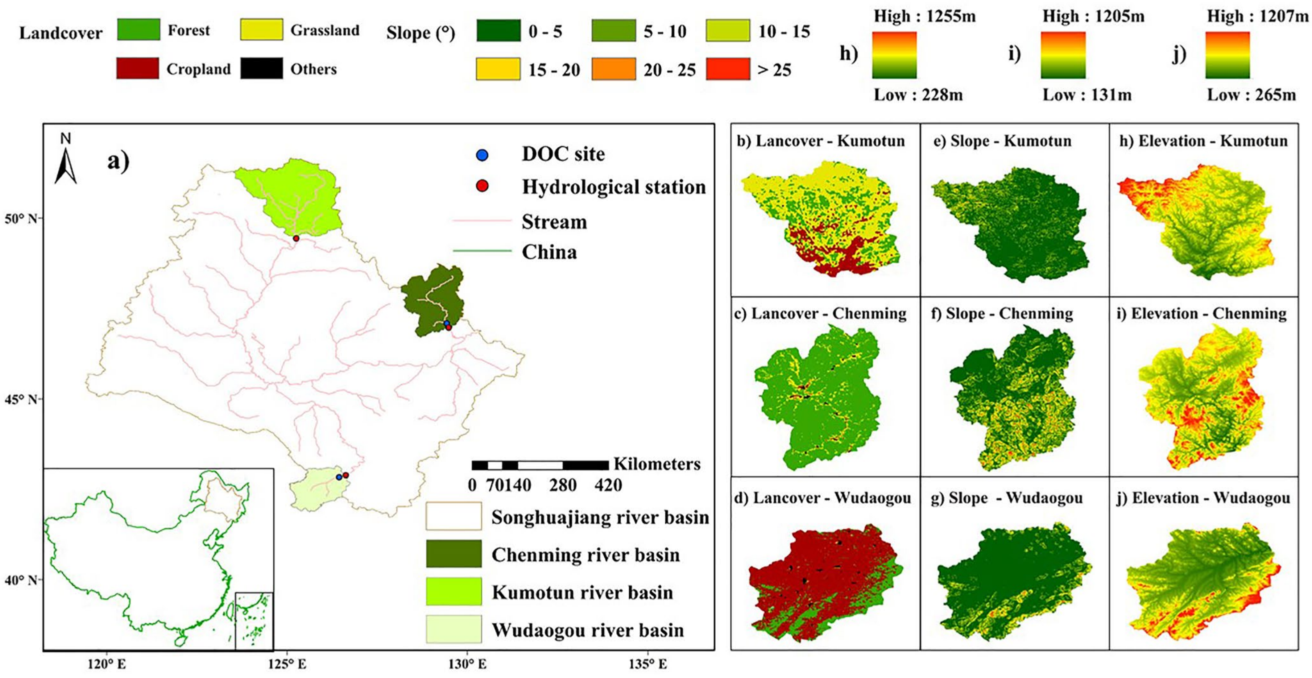

Figure 2. Spatial distribution of the three river basins investigated in this study.

3.2. Data Sets

We produced at gridded daily meteorological data set (temperature, cloud fraction, relative humidity, and wind speed) in Yuan et al. (2014) to drive the model. This data set was based on meteorological observations from 735 stations from the National Climate Center of China Meteorological Administration and was interpolated to a gridded climate data set with a spatial resolution of 10 km × 10 km using thin plate smoothing splines (Yuan et al., 2014). To reduce the simulation uncertainties of the hydrological model, this study used hourly gridded precipitation products, which were obtained from the China Meteorological Data Center (http://data.cma.cn). The data set used an optimal interpolation method to combine the inverse precipitation of the satellite-based CMORPH product (Climate Prediction Center morphing technique) and precipitation observations at more than 30,000 meteorology sites in China, and provides hourly precipitation rates at 0.1° × 0.1° starting from 2008 over the entire region of China.

The soil characteristic data were obtained from SoilGrids, a global soil property data set (https://soilgrids.org/), and included soil clay, silt, sand, bulk density, and soil organic carbon content. The ISRIC SoilGrids data set is a system for global digital soil mapping that uses state-of-the-art machine learning methods to map the spatial distribution of soil properties across the globe. The Vegetation types were classified using the Terra and Aqua combined Moderate Resolution Imaging Spectroradiometer (MODIS) Land Cover Type (MCD12Q1) Version 6 data (https://lpdaac.usgs.gov/products/mcd12q1v006). A digital elevation model (DEM) with at the spatial

Table 1
Basic Information for Three River Basins During the Periods 2008–2016

	Vegetation type (%)							
River basin	Forest	Grass	Crop	Others	Area (km^2)	Slope (degree)	Tem (°C)	Prec (mm)
Chenming	90.43	8.28	0.54	0.75	19,294	6.5	1.6	581
Kumotun	23.14	60.71	16.07	0.08	32,131	3.9	−0.1	457
Wudaogou	20.49	0.43	77.85	1.23	12,439	3.5	5.4	639

Note. Tem: mean annual temperature; Prec: annual precipitation.

resolution of 0.00833° × 0.00833° was obtained from Shuttle Elevation Derivatives at multiple scales (HydroSHEDS) data (www.hydrosheds.org), which generated the river basin boundaries, slope, and flow direction.

We collected monthly observations of streamflow and sediment loads from to 2008–2016 at three hydrological stations (Chenming, Wudaogou, and Kumotun) from the hydrological year book (Ministry of Water Resources of PRC, 2008–2016). In addition, in Chenming and Wudaogou River Basins, the riverine DOC and POC were measured at monthly intervals during the period of 2014–2016, when the water levels were not markedly different. Meanwhile, we also randomly selected sample sites on the land of these two river basins to collect DOC and SOC in 0–10 cm soil surface. Soil samples were dissolved in pure water and the solution along with river water samples was stored at in a refrigerator at under −5°C for less than 7 days, and was transferred to a laboratory using a cooler at 0°C. DOC and SOC were measured by high temperature potassium dichromate oxidation capacity. POC was hydrolyzed with NaPO3, passed through a sieve of 53 μm, and dried at 65°C.

3.3. Model Simulation

The IBIS simulation includes spin-up and transient runs. In the spin-up run, we used climate data (air temperature, relative humidity, precipitation, wind speed, air pressure, and radiation) from the early decades of the 20th century (i.e., 1901–1920) to achieve an equilibrium state of the vegetation and soil pools. The criterion for the attainment of an equilibrium state is that the differences in the average SOC and vegetation biomass over 20 recycling years are less than 5%. We used the Climatic Research Unit (CRU, v3.24) data set to drive the model. In addition, based on the CRU data set, we conducted a 40-year transient model run from 1921 to 1960 to reproduce the variations in ecosystems. Subsequently, the interpolated climate data set (from Yuan et al. (2014)) was used to drive the model from 1961 to 2018 because it has a higher spatial resolution and better performance for representing variations in meteorological variables. The carbon cycling module of IBIS was driven on a daily time step and 10 × 10 km spatial resolution, and the CRU data set was resampled into a 10 × 10 km spatial resolution. To further reduce the simulation uncertainties for hydrological processes resulting from forcing the data, we used an hourly precipitation data set (i.e., CMORPH product) to drive the hydrology module from 2008 to 2018, that is, simulated the river runoff and sediment loads (see the above section). In addition, we ran the hydrology module with a spatial resolution of 1 × 1 km, and all the driving data were resampled to 1 × 1 km.

The hydrological module and carbon cycling module have been fully coupled in this study (Figure 1). The hydrological module simulates the variables of hydrological processes at 1 × 1 km spatial resolution and hourly temporal resolution, but only provides several important variables (i.e., soil moisture) for the carbon cycle module of IBIS by aggregating it into a daily and 10 × 10 km resolution in order to match the spatial and temporal resolution of the IBIS carbon cycle module. The carbon cycle module of IBIS provides the LAI, SOC, and DOC for the hydrology module at daily and 10 × 10 km resolution, and all hydrological pixels within 10 × 10 km have the same simulations of LAI, SOC, and DOC.

3.4. Statistics Analysis

Three metrics were used to evaluate the model performance in this study:

1. The coefficient of determination, R^2, representing the variation in the observations, was explained by the model.
2. The predictive error (bias), quantifying the difference between simulated and observed values.

$$\mathrm{Bias} = \frac{\sum_{i=1}^{n}\left(Y_i^{\mathrm{sim}} - Y_i^{\mathrm{obs}}\right)}{\sum_{i=1}^{n} Y_i^{\mathrm{obs}}} \times 100\% \tag{26}$$

where Y_i^{obs} is the observed value in the ith month and Y_i^{sim} is the simulated value in the ith month.

3. The Nash-Sutcliffe Efficiency (NSE), indicating the residual variance of the simulated and observed data compared to the observed data variance (Nash & Sutcliffe, 1970).

10.1029/2023MS003916

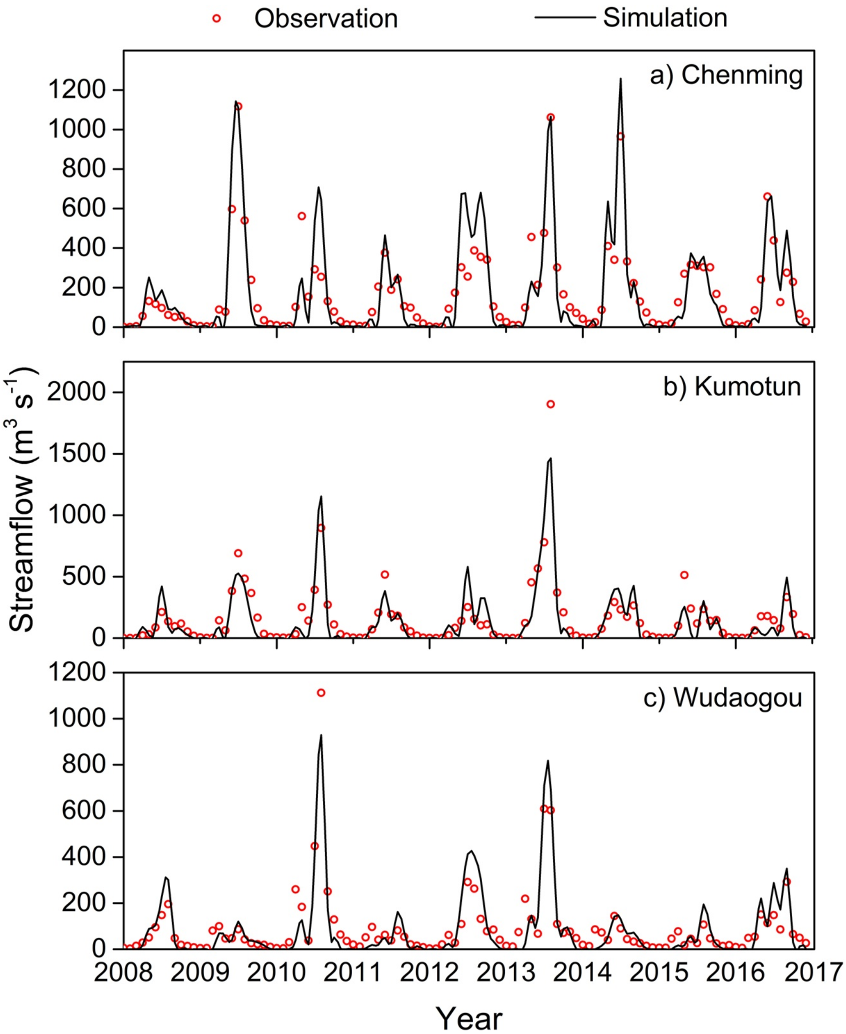

Figure 3. Observed and simulated monthly runoff in three river basins during the period of 2008–2016.

$$\mathrm{NSE} = 1 - \left[\frac{\sum_{i=1}^{n}\left(Y_i^{\mathrm{obs}} - Y_i^{\mathrm{sim}}\right)^2}{\sum_{i=1}^{n}\left(Y_i^{\mathrm{obs}} - Y^{\mathrm{mean}}\right)^2}\right] \tag{27}$$

where Y^{mean} is the mean value of the observations; and n is the total number of observations.

4. Results

4.1. Evaluations of River Runoff and Suspended Sediment

The model performances of the runoff and sediment load simulations were evaluated based on the monthly observations at three hydrological stations (Chenming, Kumotun, and Wudaogou) from 2008 to 2016 (Figure 2). As shown in Figure 3, the observed and simulated streamflow were consistent in magnitude and variation. On average, the simulated mean streamflow over the three basins were 168.85, 130.83, and 83.35 m^3 s^{-1} at Chenming, Kumotun and Wudaogou, respectively, which were close to the magnitude of the observations, with the absolute predictive error (Bias) varying from 0.49% to 12.00% (Table 2). The seasonality of the simulated streamflow was consistent with the observations at all three basins, and the R^2 and NSE were larger than 0.8 (Figure 3 and Table 2). Most of the disagreements between simulations and observations occurred in March and April.

Table 2
Evaluation Metrics of Monthly Streamflow, Sediment Load, Riverine Dissolved Organic Carbon, and Particulate Organic Carbon in the Three River Basins During the Period From 2008 to 2016

Basins	Obs.[a]	Sim.[b]	R^2	Bias (%)	NSE
Runoff ($m^3\ s^{-1}$)					
Chenming	169.67	168.85	0.82	−0.49	0.82
Kumotun	149.76	130.83	0.83	−12.00	0.81
Wudaogou	87.04	83.35	0.85	−4.24	0.85
Suspended sediment (t)					
Chenming	24,891.10	27,786.57	0.69	11.63	0.69
Kumotun	58,359.44	46,215.16	0.94	−20.81	0.66
Wudaogou	129,346.58	173,591.43	0.74	34.21	0.72
Riverine dissolved organic carbon (mg C L^{-1})					
Chenming	9.06	8.22	0.38	−9.24	0.29
Wudaogou	3.89	3.85	0.37	−1.05	0.36
Riverine particulate organic carbon (mg C L^{-1})					
Chenming	4.57	3.83	0.33	−16.09	0.14
Wudaogou	33.18	41.83	0.47	26.06	0.25

Note. a and b indicate the averaged observations and simulations of streamflow, sediment load, riverine dissolved organic carbon and riverine particulate organic carbon.

The model predictions matched the observations of the sediment load (Figure 4). The simulated annual total sediment loads at Chenming, Kumotun, and Wudaogou were 2.78×10^4 t yr^{-1}, 4.62×10^4 t yr^{-1}, and 17.35×10^4 t yr^{-1}. Our estimations were comparable overall to the observations for each basin (2.49×10^4 t yr^{-1}, 5.84×10^4 t yr^{-1},and 12.93×10^4 t yr^{-1} at Chenming, Kumotun, and Wudaogou, respectively). In general, the sediment load simulations were satisfactory in the three river basins (NSE > 0.66, $R^2 > 0.69$), and the simulations at Wudaogou site were the best (NSE = 0.72, $R^2 = 0.74$) (Table 2). The model tended to underestimate the sediment load over all three river basins, and the largest underestimation was found in the Wudaogou site in 2010 (Figure 4c, Table 2).

4.2. Validation of SOC Stocks and Fluxes in Land and Rivers

We compared the simulated SOC stocks with the observational data. The simulated average SOC stock was high in the Chenming River Basin (75.67 kg C m^{-2}), medium in the Kumotun River Basin (63.64 kg C m^{-2}) and low in Wudaogou River Basin (33.14 kg C m^{-2}) (Figure 5). Although the simulated spatial variation of the SOC stocks cannot be strictly compared to the SOC stocks derived from ISRIC SoilGrids data set, the simulated average SOC stock in these three basins were close to the SoilGrids data set (71.08, 53.16, and 39.41 kg C m^{-2} in Chenming, Kumotun, and Wudaogou, respectively).

Based on the observations of DOC in the forest (i.e., Chenming) and cropland (i.e., Wudaogou) sites, we examined the performance of revised IBIS for reproducing the DOC concentrations in soil. In general, the revised IBIS was capable of reproducing the DOC concentrations at two tested sites (Figure 6). For Chenming, the simulated average values were close to observed values, but underestimated the peak values of DOC in soil (Figure 6a). For Wudaogou, the modeled and measured values were close, but strongly underestimated DOC of 2014 (Figure 6b). On contrary, the original IBIS used a fixed DOC/SOC ratio (0.015) to simulate soil DOC content based on the simulated SOC. Figure 6 showed the very weak and contrary seasonal variations of simulated DOC compared to observed DOC, and the magnitude of simulated DOC were also quite higher than the observations (Figure 6).

The model was able to simulate the temporal and spatial variations of riverine DOC and POC concentrations in both the Chenming and Wudaogou basins (Figure 7). Our simulation reproduced the observed seasonal variations in the observed riverine DOC concentrations in these two basins (Figures 7a, 7c). The average prediction errors at Chenming and Wudaogou were −9.24% and −1.05%, respectively (Table 2). Compared with the DOC simulations, there were relatively larger uncertainties in the simulated riverine POC concentrations, with average errors of 16.09% and 26.06% at Chenming and Wudaogou, respectively (Table 2).

4.3. Spatial Patterns of SOC Erosion and Deposition

The soil and SOC erosion and deposition of the three studied river basins were simulated by this coupling model in 2008–2016, especially considering SOC lateral and vertical movement. The spatial distributions of the average annual soil erosion and deposition rate (Figures 8a–8c) were similar to the spatial distributions of the slope (Figures 2b–2d). The highest soil erosion rates occurred in the high-slope regions. The spatial distributions of SOC erosion and deposition were consistent with those of soil erosion and deposition (Figures 8d–8f).

Moreover, we compared the SOC in the top 5 cm soil layer simulated by the revised IBIS model with the soil erosion process to that simulated by the original IBIS model without erosion in 2008–2016 (Figure 9). The net soil and SOC erosion were 16.68 g m^{-2} yr^{-1} and 0.26 g C m^{-2} yr^{-1} in the Chenming (forest) River Basin, 17.28 g m^{-2} yr^{-1} and 0.22 g C m^{-2} yr^{-1} in the Kumotun (grassland) River Basin and 167.42 g m^{-2} yr^{-1} and 1.68 g C m^{-2} yr^{-1} in the Wudaogou (cropland) River Basin, respectively (Figures 9a–9f). Compared to the original IBIS model without soil erosion process, the SOC stocks decreased by 12.06, 16.02, and 64.98 g C m^{-2} in revised IBIS model with the soil erosion process (Figures 9g–9i). In addition, the gross SOC erosion was 1.34,

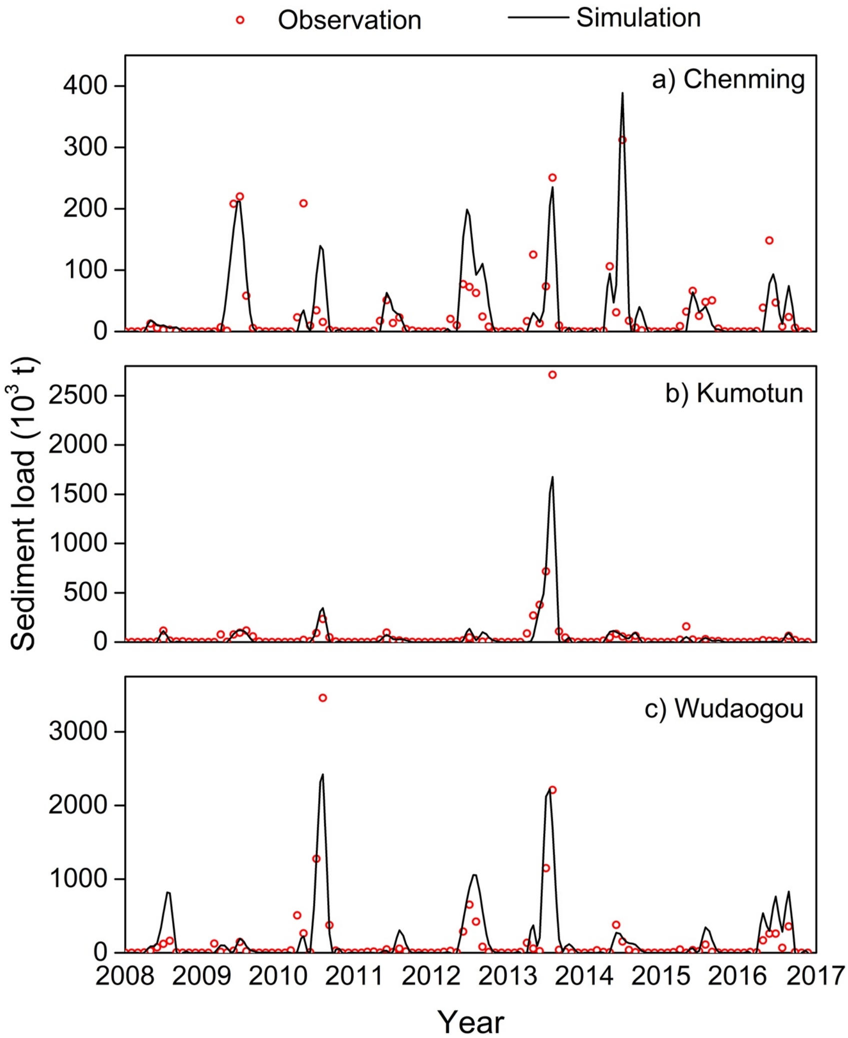

Figure 4. Observed and simulated monthly sediment load in the three river basins during the period of 2008–2016.

1.78, and 7.22 g C m^{-2} yr^{-1} in the Chenming, Kumotun and Wudaogou River Basins, which were equal to 0.27%, 0.35%, and 1.45% of the NPP (493.73, 501.77, and 498.62 g C m^{-2} yr^{-1}) in the corresponding basins, respectively.

4.4. Impacts of Land Cover on Lateral Movements of SOC

Both observations and simulations highlighted large differences in the lateral movements of SOC among three river basins. On average, the Wudaogou River Basin, covered majorly by cropland, showed the largest suspended sediment compared to the Chenming (dominated by forest) and Kumotun (dominated by grassland) River Basins (Table 2). The ratio of suspended sediment and river basin area over the Wudaogou River Basin is 8.06 and 5.72 times than those of Chenming and Kumotun, respectively (Figure 10a). In addition, the ratio between annual suspended sediment and runoff also showed the largest at the cropland dominated basin (i.e., Wudaogou River Basin), and the lowest at the forest dominated based (i.e., Chenming River Basin) (Figure 10b). Consequently, Wudaogou River Basin showed the larger riverine POC content than Chenming River Basin (Table 2). However, riverine DOC at Chenming River Basin was higher than Wudaogou River Basin (Table 2).

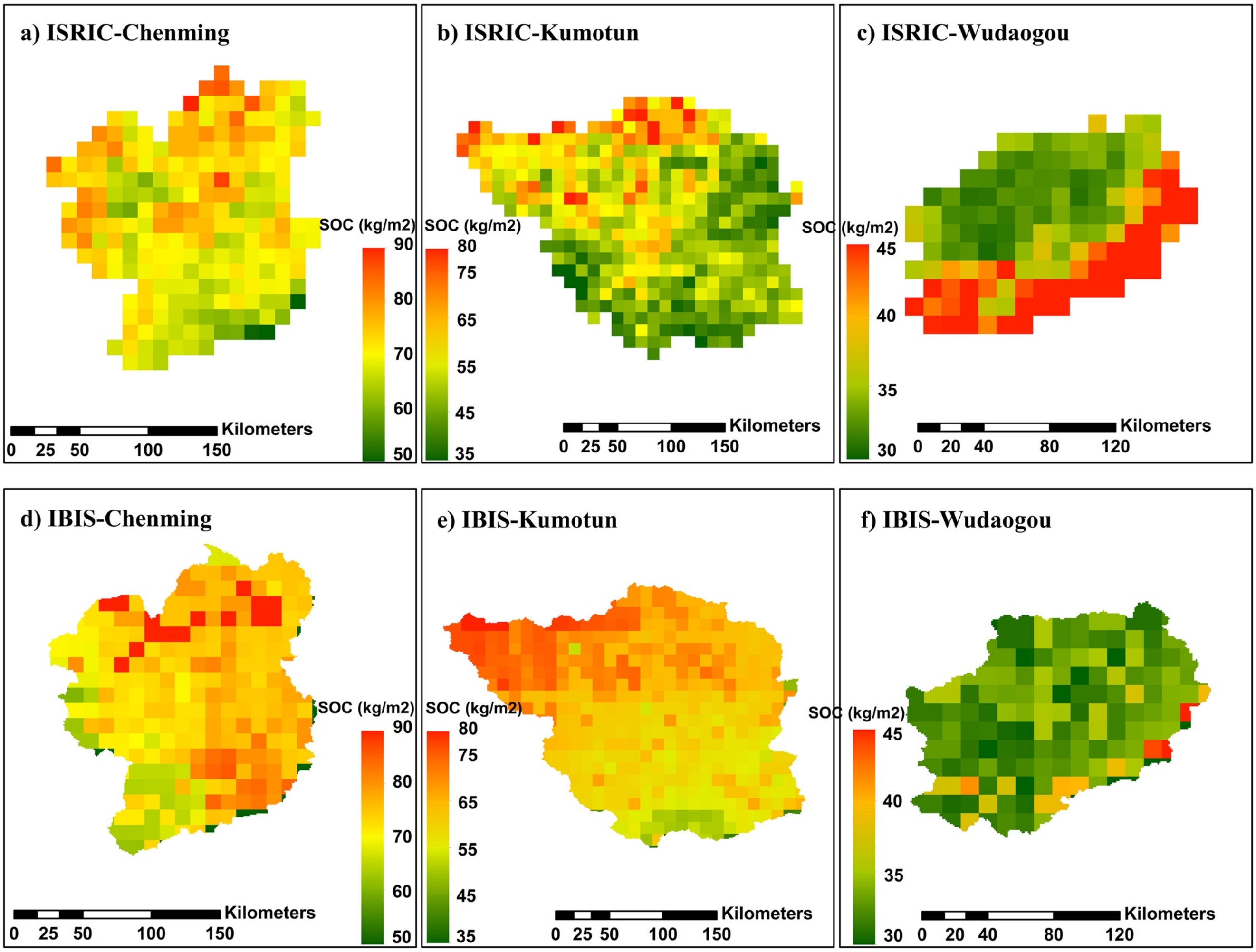

Figure 5. Comparison of the soil organic carbon (SOC) stocks in the two m soil layer derived from the ISRIC SoilGrids data set (a–c) and IBIS model (d–f).

5. Discussion

5.1. Model Performance and Implications

In our study, we incorporated new soil carbon processes into an ecosystem model (i.e., IBIS), with a full coupling between soil carbon lateral movements and hydrological processes, and explicitly represented the erosion and deposition of SOC within the land surface and rivers. The newly developed model captured changes in runoff, sediment loads, soil DOC concentration and riverine DOC and POC in three river basins in Northeast China, which were dominated by three different vegetation types. In addition to the validations of the integrated model against the measured river runoff and sediment loads (Figures 3 and 4; Table 2), a comparison between this study and previous studies also indicates the reasonability of our model. Based on the second national soil erosion survey data set that was taken in 2010–2012 (Wang et al., 2019; Yue et al., 2016), the magnitude of total soil erosion was 0.87, 2.67, and 10.64 Tg yr^{-1} within the Chenming, Kumotun and Wudaogou basins, respectively, which were quite close to our estimates.

Our results demonstrated that the annual SOC lateral movement by erosion was equivalent to 0.27%–1.45% of the annual vegetation NPP. This was close to the estimate (0.55%) made for the European Rhine Basin (Zhang et al., 2020). Other studies have shown that terrestrial organic carbon delivered into the aquatic ecosystem is approximately 0.5%–2% of the NPP (Wang et al., 2015; Zhang et al., 2020), and the carbon sink induced by erosion is likely to be 1% of the NPP (Berhe et al., 2007). As a result, erosion redistribution is crucial for quantifying the effect of erosion on the carbon cycle.

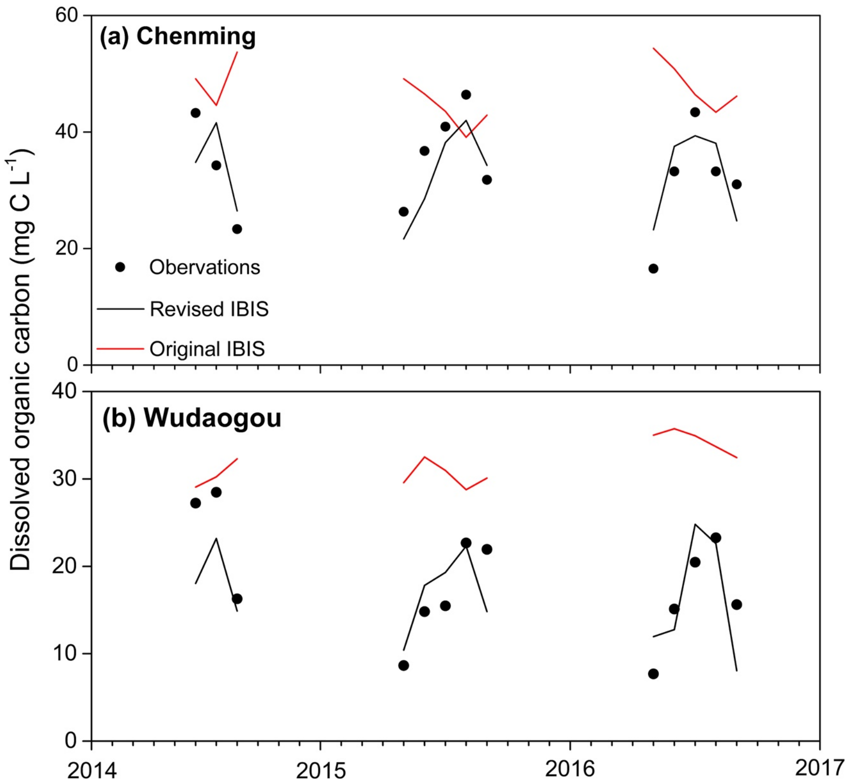

Figure 6. Observed and simulated concentration of dissolved organic carbon (mg C L^{-1}) in 0–10 cm depth of soil at Chenming (a) and Wudaogou (b) river basins. The black dots indicate the observations and the lines indicate the simulations.

5.2. Impacts of Land Cover on SOC Erosion

Our simulations showed substantial differences on the eroded soil sediment and SOC in the three river basins that dominated by different vegetation types. The eroded soil and SOC of the Wudaogou River Basin, dominated by cropland, were distinctly larger than those of the other two basins at the same precipitation level (Table 2). Other lines of evidence support the conclusion that cropland ecosystems have higher soil erosion rates than other natural ecosystems. For example, in Australia, the sediment yield for the grazed pasture and forest/woodland basins did not exceed 2.2 and 0.8 ton ha^{-1} yr^{-1}, respectively; however, cultivated land produced as much as 3.1 ton ha^{-1} yr^{-1} (Erskine et al., 2002). Compared with forest and grassland, the POC export with the sediment load in cropland ecosystems was higher because of the lower rates of interception and the surface soil that was not covered by plants was subjected to the direct impacts of rain (Fohrer et al., 2001).

Both observations and simulations showed larger DOC concentrations in the soil and rivers over the basin dominated by forest ecosystems (i.e., Chenming River Basin) relative to the basin dominated by cropland ecosystems (Table 2). A recent study in the adjacent river basins supported our conclusion and provided evidence that the DOC concentration in the soil of forested ecosystems is higher than that in cropland (Wang et al., 2020). Previous studies have highlighted at larger SOC removal in the form of POC from terrestrial to aquatic ecosystems in croplands than in natural ecosystems (Chappell et al., 2016). Our results demonstrated that more attention should be paid to the fluvial transport of DOC from forest ecosystems. In particular, the decomposition rate of DOC is faster than that of POC, which leads to higher carbon emissions (Cole et al., 2007).

5.3. Model Limitations

The DOC sorption and desorption in the soil are two key processes related to the DOC concentrations in soil solutions. Our model used a simplified method to represent the DOC sorption process. However, when DOC

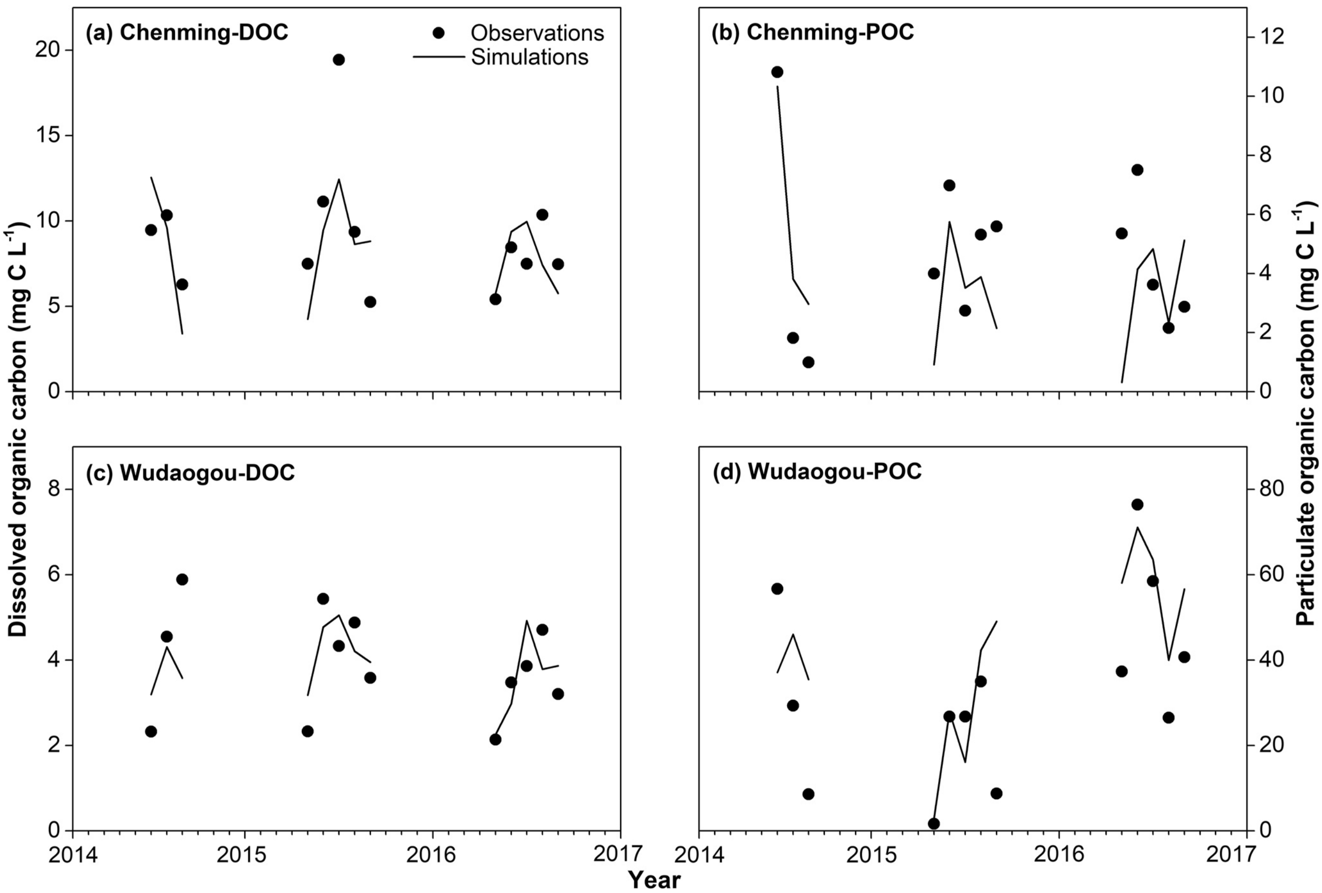

Figure 7. Riverine dissolved organic carbon (DOC) and particulate organic carbon (POC) concentrations (mg C L^{-1}) at Chenming (a), (b) and Wudaogou (c), (d) river basins. The black dots indicate the observations and the lines indicate the simulations.

percolates in the soil profile, it may interact with metal oxide surfaces, thereby forming a "shield" against microbial attack (Blaser et al., 1994). In acidic forest soils, Al and Fe can form relatively stable complexes with DOC, which can enhance the solubility and transport (Jansen et al., 2005). This study did not integrate the impacts of metal oxides on DOC sorption because the processes of Al and Fe in soils are currently lacking. Our results also highlight that coupling of the carbon cycle with other biogeochemical variables is important for improving simulations of the carbon flux in terrestrial ecosystems.

This study used a fixed POC content of riverine suspended sediment to simulate fluvial POC export. However, a recent study reported a decline in the POC concentration with an increase in suspended sediment (Ran et al., 2020). Our study, using a constant POC concentration, may result in uncertainties in the seasonal variations in POC exports. Future model improvements need to consider temporal changes in the POC concentration. In addition, previous studies have shown that the seasonal variation in POC concentration is primarily derived from modern soils and terrestrial C3 plant litterfall (Liu et al., 2003). Our model did not include POC sources from plant litterfall. Several studies have also shown a lower degradation efficiency of POC with fine silt and clay sediment particles; therefore, the POC content usually decreases with an increasing grain size of the sediment aggregates (Zhang et al., 2013). Additionally, in this study, we assumed that the land-river lateral movement of organic carbon is a teleportation process, also including the teleport of carbon from grid cells that are not adjacent to a river cell. Soil texture and particle sizes can impact on the teleport and deposition processes of POC. Separating particle sizes in future models may be beneficial for simulating POC exports.

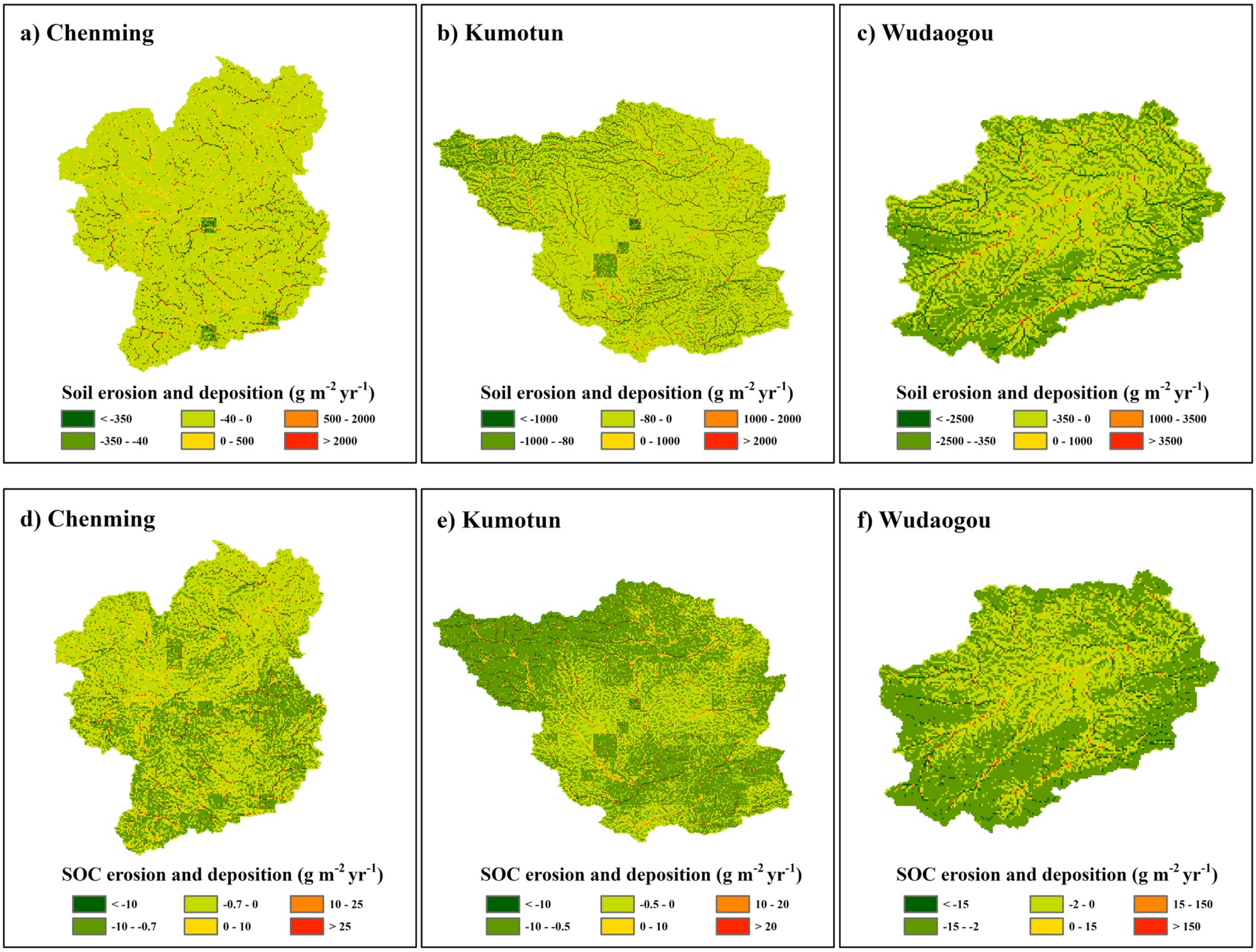

Figure 8. Spatial distributions of the average annual erosion and deposition rate of soil (a–c) and soil organic carbon (SOC) (d–f) during 2008–2016 at 1 × 1 km spatial resolution.

6. Conclusions

In this study, we developed a new model for simulating the lateral transfer of DOC and POC from land to rivers, and integrated this into a terrestrial ecosystem model (IBIS). The new model fully considered DOC production, vertical evolution of SOC, and the transport processes to rivers. The coupling model was applied at a 1 km resolution in the Chenming, Kumotun, and Wudaogou River Basins with different land covers in 2008–2016. The evaluations of the streamflow and sediment load demonstrated a satisfactory performance of our model. Our results showed that the spatial distributions of the soil and SOC erosion and deposition, and the estimated annual eroded SOC movement is 0.27%–1.45% of the annual NPP. The soil and SOC erosion in farmland was greater than that in grassland and forest. The redistributed proportions of erosion in farmland were higher than those in grassland and forest. The new process-based model is an attempt to incorporate the lateral transfer of organic carbon into the terrestrial ecosystem model. In the future, more observations and further improvements of our model will help to reduce the uncertainties in the predicted ecosystem carbon cycle.

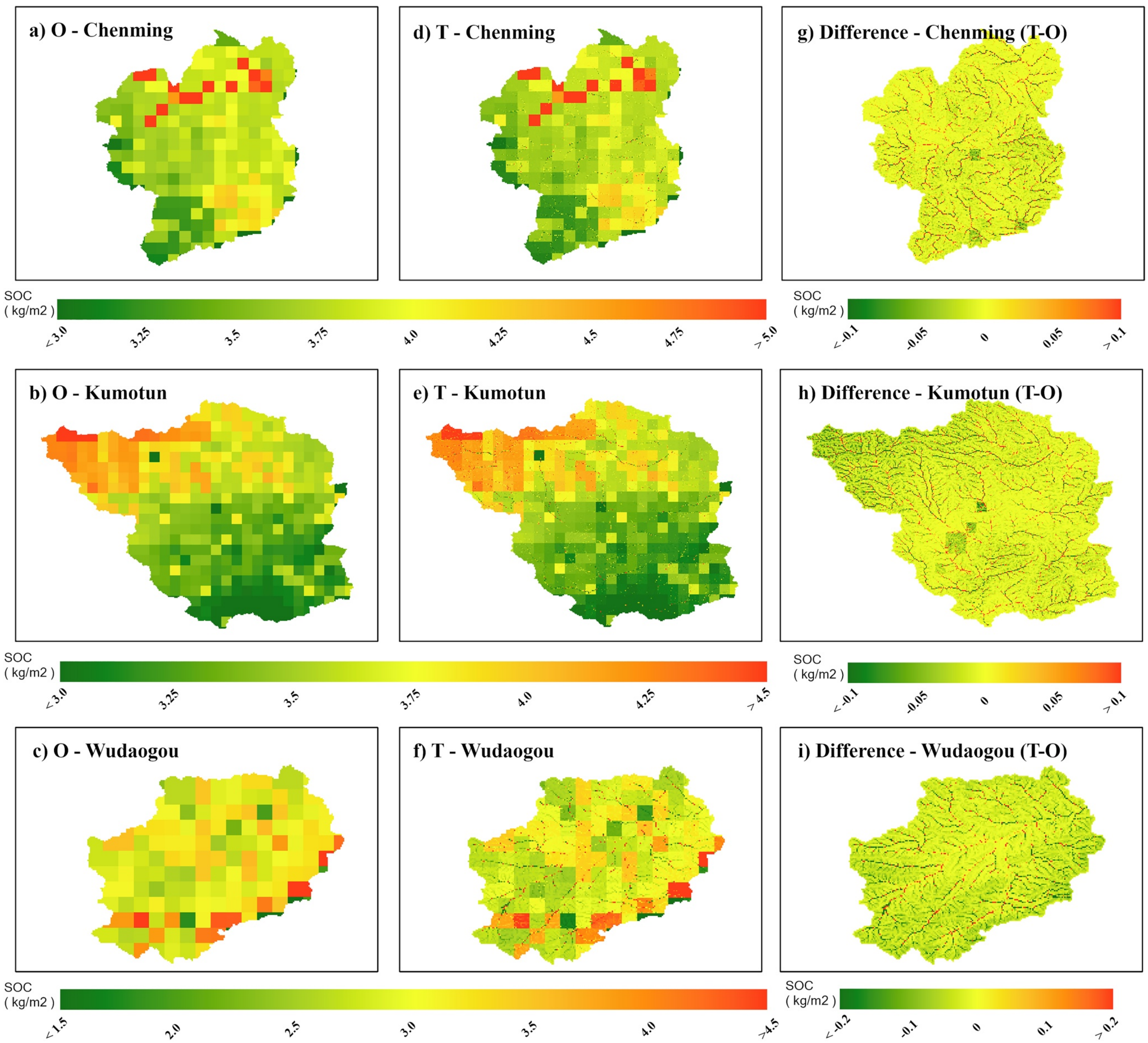

Figure 9. Comparison of the soil organic carbon (SOC) stocks in the top 5 cm soil layer at 1 × 1 km spatial resolution simulated by the original IBIS (O) (a–c) and revised IBIS with soil erosion processes (T) (d–f). (g)–(i) indicate the differences (T–O) of simulated SOC between the original IBIS (O) and revised IBIS (T).

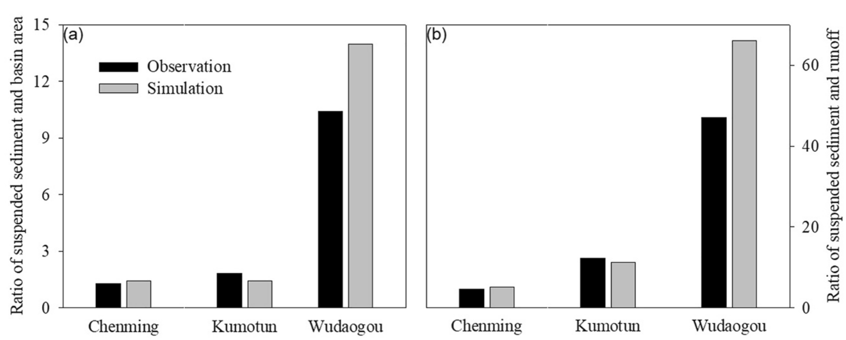

Figure 10. Comparison of ratio of annual suspended sediment (g) and basin area (m^2) (a) and runoff (m^3) (b).

Data Availability Statement

The observed and simulated runoff, sediment, DOC, POC, soil, and SOC erosion data set and the source code of the integrated model are available via the repository (Lu & Yuan, 2023). All input data sets driving the models in this study are publicly accessible online. The gridded daily meteorological data set used for driving the model has been published by Yuan et al. (2014). The soil characteristic data were obtained from the SoilGrids data set (Batjes et al., 2020). The vegetation type data was from classified the MODIS Land Cover Type (MCD12Q1) Version 6 data set, can be downloaded at the USGS EarthData Repository (Sulla-Menashe & Friedl, 2018). A digital elevation model can be obtained from the HydroSHEDS data set (Lehner et al., 2021).

Acknowledgments
This research was funded by the National Natural Science Foundation of China for Distinguished Young Scientists (41925001), National Natural Science Foundation of China (42101026, 42141020, 31930072), and Guangdong Basic and Applied Basic Research Foundation (2020A1515111145).

References

Alberts, E. E., Nearing, M., Weltz, M., Risse, M., Pierson, F., Zhang, X. C., et al. (1995). Soil component. In *USDA-water erosion prediction project: Hillslope profile and watershed model Documentation*. NSERL Report. Retrieved from https://www.ars.usda.gov/midwest-area/west-lafayette-in/national-soil-erosion-research/docs/wepp/wepp-model-documentation/

Baetz, U., & Martinoia, E. (2014). Root exudates: The hidden part of plant defense. *Trends in Plant Science*, *19*(2), 90–98. https://doi.org/10.1016/j.tplants.2013.11.006

Bantle, A., Borken, W., Ellerbrock, R. H., Schulze, E. D., Weisser, W. W., & Matzner, E. (2014). Quantity and quality of dissolved organic carbon released from coarse woody debris of different tree species in the early phase of decomposition. *Forest Ecology and Management*, *329*, 287–294. https://doi.org/10.1016/j.foreco.2014.06.035

Batjes, N. H., Ribeiro, E., & van Oostrum, A. (2020). Standardised soil profile data to support global mapping and modelling (WoSIS snapshot 2019) [Dataset]. Earth System Science Data, *12*(1), 299–320. https://doi.org/10.5194/essd-12-299-2020

Batson, J., Noe, G. B., Hupp, C. R., Krauss, K. W., Rybicki, N. B., & Schenk, E. R. (2015). Soil greenhouse gas emissions and carbon budgeting in a short-hydroperiod floodplain wetland. *Journal of Geophysical Research: Biogeosciences*, *120*(1), 77–95. https://doi.org/10.1002/2014jg002817

Battin, T. J., Luyssaert, S., Kaplan, L. A., Aufdenkampe, A. K., Richter, A., & Tranvik, L. J. (2009). The boundless carbon cycle. *Nature Geoscience*, *2*(9), 598–600. https://doi.org/10.1038/ngeo618

Berhe, A. A., Harte, J., Harden, J. W., & Torn, M. S. (2007). The significance of the erosion-induced terrestrial carbon sink. *BioScience*, *57*(4), 337–346. https://doi.org/10.1641/b570408

Blaser, P., Senesi, N., & Miano, T. M. (1994). The role of natural organic matter in the dynamics of metals in forest soils. In *Humic substances in the global environment and implications on human health* (pp. 943–960). Elsevier.

Bolan, N. S., Adriano, D. C., Kunhikrishnan, A., James, T., McDowell, R., & Senesi, N. (2011). Dissolved organic matter: Biogeochemistry, dynamics, and environmental significance in soils. *Advances in Agronomy, 110. D. L. Sparks.*, *110*, 1–75.

Casas-Ruiz, J. P., Bodmer, P., Bona, K. A., Butman, D., Couturier, M., Emilson, E. J. S., et al. (2023). Integrating terrestrial and aquatic ecosystems to constrain estimates of land-atmosphere carbon exchange. *Nature Communications*, *14*(1), 1571. https://doi.org/10.1038/s41467-023-37232-2

Chaplot, V. A. M., Rumpel, C., & Valentin, C. (2005). Water erosion impact on soil and carbon redistributions within uplands of Mekong River. *Global Biogeochemical Cycles*, *19*(4). https://doi.org/10.1029/2005gb002493

Chappell, A., Baldock, J., & Sanderman, J. (2016). The global significance of omitting soil erosion from soil organic carbon cycling schemes. *Nature Climate Change*, *6*(2), 187–191. https://doi.org/10.1038/nclimate2829

Chen, S. Y., Cao, R. M., Yoshitake, S., & Ohtsuka, T. (2019). Stemflow hydrology and DOM flux in relation to tree size and rainfall event characteristics. *Agricultural and Forest Meteorology*, *279*, 107–753. https://doi.org/10.1016/j.agrformet.2019.107753

Cole, J. J., Prairie, Y. T., Caraco, N. F., McDowell, W. H., Tranvik, L. J., Striegl, R. G., et al. (2007). Plumbing the global carbon cycle: Integrating inland waters into the terrestrial carbon budget. *Ecosystems*, *10*(1), 172–185. https://doi.org/10.1007/s10021-006-9013-8

Davidson, E. A., & Janssens, I. A. (2006). Temperature sensitivity of soil carbon decomposition and feedbacks to climate change. *Nature*, *440*(7081), 165–173. https://doi.org/10.1038/nature04514

Dick, J. J., Tetzlaff, D., Birkel, C., & Soulsby, C. (2015). Modelling landscape controls on dissolved organic carbon sources and fluxes to streams. *Biogeochemistry*, *122*(2–3), 361–374. https://doi.org/10.1007/s10533-014-0046-3

Erskine, W. D., Mahmoudzadeh, A., & Myers, C. (2002). Land use effects on sediment yields and soil loss rates in small basins of Triassic sandstone near Sydney, NSW, Australia. *Catena*, *49*(4), 271–287. https://doi.org/10.1016/s0341-8162(02)00065-6

Fohrer, N., Haverkamp, S., Eckhardt, K., & Frede, H. G. (2001). Hydrologic response to land use changes on the catchment scale. *Physics and Chemistry of the Earth - Part B: Hydrology, Oceans and Atmosphere*, *26*(7–8), 577–582. https://doi.org/10.1016/s1464-1909(01)00052-1

Futter, M. N., Butterfield, D., Cosby, B. J., Dillon, P. J., Wade, A. J., & Whitehead, P. G. (2007). Modeling the mechanisms that control in-stream dissolved organic carbon dynamics in upland and forested catchments. *Water Resources Research*, *43*(2). https://doi.org/10.1029/2006wr004960

Galy, V., Peucker-Ehrenbrink, B., & Eglinton, T. (2015). Global carbon export from the terrestrial biosphere controlled by erosion. *Nature*, *521*(7551), 204–207. https://doi.org/10.1038/nature14400

Guillaume, T., Damris, M., & Kuzyakov, Y. (2015). Losses of soil carbon by converting tropical forest to plantations: Erosion and decomposition estimated by $\delta^{13}C$. *Global Change Biology*, *21*(9), 3548–3560. https://doi.org/10.1111/gcb.12907

Hagedorn, F., Saurer, M., & Blaser, P. (2004). A C-13 tracer study to identify the origin of dissolved organic carbon in forested mineral soils. *European Journal of Soil Science*, *55*(1), 91–100. https://doi.org/10.1046/j.1365-2389.2003.00578.x

Harrison, A. F., Taylor, K., Scott, A., Poskitt, J., Benham, D., Grace, J., et al. (2008). Potential effects of climate change on DOC release from three different soil types on the northern Pennines UK: Examination using field manipulation experiments. *Global Change Biology*, *14*(3), 687–702. https://doi.org/10.1111/j.1365-2486.2007.01504.x

Hilton, R. G., Galy, A., Hovius, N., Kao, S. J., Horng, M.-J., & Chen, H. (2012). Climatic and geomorphic controls on the erosion of terrestrial biomass from subtropical mountain forest: Erosion of carbon from mountain forest. *Global Biogeochemical Cycles*, *26*(3), GB3014. https://doi.org/10.1029/2012GB004314

Högberg, M. N., & Högberg, P. (2002). Extramatrical ectomycorrhizal mycelium contributes one-third of microbial biomass and produces, together with associated roots, half the dissolved organic carbon in a forest soil. *New Phytologist*, *154*(3), 791–795. https://doi.org/10.1046/j.1469-8137.2002.00417.x

Iavorivska, L., Boyer, E. W., & DeWalle, D. R. (2016). Atmospheric deposition of organic carbon via precipitation. *Atmospheric Environment*, *146*, 153–163. https://doi.org/10.1016/j.atmosenv.2016.06.006

Inamdar, S., Finger, N., Singh, S., Mitchell, M., Levia, D., Bais, H., et al. (2012). Dissolved organic matter (DOM) concentration and quality in a forested mid-Atlantic watershed, USA. *Biogeochemistry*, *108*(1–3), 55–76. https://doi.org/10.1007/s10533-011-9572-4

IPCC. (2014). In R. K. Pachauri & L. A. Meyer (Eds.), *Climate Change 2014: Synthesis Report. Contribution of Working Groups I, II and III to the Fifth Assessment Report of the Intergovernmental Panel on Climate Change [Core Writing Team* (p. 151). IPCC. in IPCC AR5 Synthesis Report website.

Ito, A. (2007). Simulated impacts of climate and land-cover change on soil erosion and implication for the carbon cycle, 1901 to 2100. *Geophysical Research Letters*, *34*(9), L09403. https://doi.org/10.1029/2007GL029342

Jansen, B., Nierop, K. G. J., & Verstraten, J. M. (2005). Mechanisms controlling the mobility of dissolved organic matter, aluminium and iron in podzol B horizons. *European Journal of Soil Science*, *56*(4), 537–550. https://doi.org/10.1111/j.1365-2389.2004.00686.x

Jenson, K., & Domingue, O. (1988). Extracting topographic structure from digital elevation data for geographic system analysis. *Photogrammetric Engineering & Remote Sensing*, *54*.

Jeong, J. J., Bartsch, S., Fleckenstein, J. H., Matzner, E., Tenhunen, J. D., Lee, S. D., et al. (2012). Differential storm responses of dissolved and particulate organic carbon in a mountainous headwater stream, investigated by high-frequency, in situ optical measurements: In situ monitoring of stream DOC and POC. *Journal of Geophysical Research*, *117*(G3), G03013. https://doi.org/10.1029/2012JG001999

Jones, M. B., & Donnelly, A. (2004). Carbon sequestration in temperate grassland ecosystems and the influence of management, climate and elevated CO_2. *New Phytologist*, *164*(3), 423–439. https://doi.org/10.1111/j.1469-8137.2004.01201.x

Kaiser, K., Guggenberger, G., Haumaier, L., & Zech, W. (2001). Seasonal variations in the chemical composition of dissolved organic matter in organic forest floor layer leachates of old-growth Scots pine (Pinus sylvestris L.) and European beech (Fagus sylvatica L.) stands in northeastern Bavaria, Germany. *Biogeochemistry*, *55*(2), 103–143. https://doi.org/10.1023/a:1010694032121

Kalbitz, K., Meyer, A., Yang, R., & Gerstberger, P. (2007). Response of dissolved organic matter in the forest floor to long-term manipulation of litter and throughfall inputs. *Biogeochemistry*, *86*(3), 301–318. https://doi.org/10.1007/s10533-007-9161-8

Kalbitz, K., Schwesig, D., Schmerwitz, J., Kaiser, K., Haumaier, L., Glaser, B., et al. (2003). Changes in properties of soil-derived dissolved organic matter induced by biodegradation. *Soil Biology and Biochemistry*, *35*(8), 1129–1142. https://doi.org/10.1016/s0038-0717(03)00165-2

Kalbitz, K., Solinger, S., Park, J. H., Michalzik, B., & Matzner, E. (2000). Controls on the dynamics of dissolved organic matter in soils: A review. *Soil Science*, *165*(4), 277–304. https://doi.org/10.1097/00010694-200004000-00001

Khoi, D. N., & Suetsugi, T. (2014). Impact of climate and land-use changes on hydrological processes and sediment yield—A case study of the Be River Catchment, Vietnam. *Hydrological Sciences Journal*, *59*(5), 1095–1108. https://doi.org/10.1080/02626667.2013.819433

Klotzbücher, T., Kaiser, K., Filley, T. R., & Kalbitz, K. (2013). Processes controlling the production of aromatic water-soluble organic matter during litter decomposition. *Soil Biology and Biochemistry*, *67*, 133–139. https://doi.org/10.1016/j.soilbio.2013.08.003

Kucharik, C. J., Foley, J. A., Delire, C., Fisher, V. A., Coe, M. T., Lenters, J. D., et al. (2000). Testing the performance of a Dynamic Global Ecosystem Model: Water balance, carbon balance, and vegetation structure. *Global Biogeochemical Cycles*, *14*(3), 795–825. https://doi.org/10.1029/1999gb001138

Lal, R. (2003). Soil erosion and the global carbon budget. *Environment International*, *29*(4), 437–450. https://doi.org/10.1016/s0160-4120(02)00192-7

Lal, R. (2004). Soil carbon sequestration impacts on global climate change and food security. *Science*, *304*(5677), 1623–1627. https://doi.org/10.1126/science.1097396

Lauerwald, R., Regnier, P., Camino-Serrano, M., Guenet, B., Guimberteau, M., Ducharne, A., et al. (2017). ORCHILEAK (revision 3875): A new model branch to simulate carbon transfers along the terrestrial-aquatic continuum of the Amazon basin. *Geoscientific Model Development*, *10*(10), 3821–3859. https://doi.org/10.5194/gmd-10-3821-2017

Lehner, B., Roth, A., Huber, M., Anand, M., Grill, G., Osterkamp, N., et al. (2021). HydroSHEDS v2.0—Refined global river network and catchment delineations from TanDEM-X elevation data [Dataset]. EGU General Assembly 2021, online, 19–30 Apr 2021, EGU21-9277 www.hydrosheds.org

Le Mellec, A., Meesenburg, H., & Michalzik, B. (2010). The importance of canopy-derived dissolved and particulate organic matter (DOM and POM)—Comparing throughfall solution from broadleaved and coniferous forests. *Annals of Forest Science*, *67*(4), 411. https://doi.org/10.1051/forest/2009130

Levia, D. F., & Germer, S. (2015). A review of stemflow generation dynamics and stemflow-environment interactions in forests and shrublands. *Reviews of Geophysics*, *53*(3), 673–714. https://doi.org/10.1002/2015rg000479

Levia, D. F., & Herwitz, S. R. (2000). Physical properties of water in relation to stemflow leachate dynamics: Implications for nutrient cycling. *Canadian Journal of Forest Research-Revue Canadienne De Recherche Forestiere*, *30*(4), 662–666. https://doi.org/10.1139/x99-244

Levia, D. F., Van Stan, J. T., Siegert, C. M., Inamdar, S. P., Mitchell, M. J., Mage, S. M., & McHale, P. J. (2011). Atmospheric deposition and corresponding variability of stemflow chemistry across temporal scales in a mid-Atlantic broadleaved deciduous forest. *Atmospheric Environment*, *45*(18), 3046–3054. https://doi.org/10.1016/j.atmosenv.2011.03.022

Liao, C., Zhuang, Q., Leung, L. R., & Guo, L. (2019). Quantifying dissolved organic carbon dynamics using a three-dimensional terrestrial ecosystem model at high spatial-temporal resolutions. *Journal of Advances in Modeling Earth Systems*, *11*(12), 4489–4512. https://doi.org/10.1029/2019ms001792

Liebmann, P., Wordell-Dietrich, P., Kalbitz, K., Mikutta, R., Kalks, F., Don, A., et al. (2020). Relevance of aboveground litter for soil organic matter formation—A soil profile perspective. *Biogeosciences*, *17*(12), 3099–3113. https://doi.org/10.5194/bg-17-3099-2020

Lindow, S. E., & Brandl, M. T. (2003). Microbiology of the phyllosphere. *Applied and Environmental Microbiology*, *69*(4), 1875–1883. https://doi.org/10.1128/aem.69.4.1875-1883.2003

Liu, D., Cai, W., Xia, J., Dong, W., Zhou, G., Chen, Y., et al. (2014). Global validation of a process-based model on vegetation gross primary production using eddy covariance observations. *PLoS One*, *9*(11), e110407. https://doi.org/10.1371/journal.pone.0110407

Liu, Q. M., Wang, S. J., Piao, H. C., & Ouyang, Z. Y. (2003). The changes in soil organic matter in a forest-cultivation sequence traced by stable carbon isotopes. *Australian Journal of Soil Research*, *41*(7), 1317–1327. https://doi.org/10.1071/sr03004

Lu, H., & Yuan, W. (2023). The improved terrestrial ecosystem model (IBIS) integrated with soil organic carbon lateral movement processes [Software]. Zenodo. https://doi.org/10.5281/zenodo.10004127

Lu, H., Yuan, W., & Chen, X. (2019). A processes-based dynamic root growth model integrated into the ecosystem model. *Journal of Advances in Modeling Earth Systems*, *11*(12), 4614–4628. https://doi.org/10.1029/2019MS001846

Lu, X., & Zhuang, Q. (2015). An integrated dissolved organic carbon dynamics model (DOCDM 1.0): Model development and a case study in the Alaskan Yukon River Basin. *Geoscientific Model Development Discussions*, *8*, 10411–10454. https://doi.org/10.5194/gmdd-8-10411-2015

Lynch, J. M., & Whipps, J. M. (1990). Substrate flow in the rhizosphere. *Plant and Soil*, *129*, 1–10. https://doi.org/10.1007/bf00011685

Magnússon, R. I., Tietema, A., Cornelissen, J. H. C., Hefting, M. M., & Kalbitz, K. (2016). Tamm Review: Sequestration of carbon from coarse woody debris in forest soils. *Forest Ecology and Management*, *377*, 1–15. https://doi.org/10.1016/j.foreco.2016.06.033

Manzoni, S., Taylor, P., Richter, A., Porporato, A., & Agren, G. I. (2012). Environmental and stoichiometric controls on microbial carbon-use efficiency in soils. *New Phytologist*, *196*(1), 79–91. https://doi.org/10.1111/j.1469-8137.2012.04225.x

Marschner, B., & Kalbitz, K. (2003). Controls of bioavailability and biodegradability of dissolved organic matter in soils. *Geoderma*, *113*(3–4), 211–235. https://doi.org/10.1016/s0016-7061(02)00362-2

Meyer, L. D., & Wischmeier, W. H. (1969). Mathematical simulation of the process of soil erosion by water. *Transactions of the American Society of Agricultural Engineers*, *12*, 754–758.

Michalzik, B., Kalbitz, K., Park, J. H., Solinger, S., & Matzner, E. (2001). Fluxes and concentrations of dissolved organic carbon and nitrogen—A synthesis for temperate forests. *Biogeochemistry*, *52*, 172–205.

Michalzik, B., Levia, D. F., Bischoff, S., Naethe, K., & Richter, S. (2016). Effects of aphid infestation on the biogeochemistry of the water routed through European beech (Fagus sylvatica L.) saplings. *Biogeochemistry*, *129*(1–2), 197–214. https://doi.org/10.1007/s10533-016-0228-2

Moore, T. R. (2003). Dissolved organic carbon in a northern boreal landscape. *Global Biogeochemical Cycles*, *17*(4). https://doi.org/10.1029/2003gb002050

Moore, T. R., Pare, D., & Boutin, R. (2008). Production of dissolved organic carbon in Canadian forest soils. *Ecosystems*, *11*(5), 740–751. https://doi.org/10.1007/s10021-008-9156-x

Mueller, M., Alewell, C., & Hagedorn, F. (2009). Effective retention of litter-derived dissolved organic carbon in organic layers. *Soil Biology and Biochemistry*, *41*(6), 1066–1074. https://doi.org/10.1016/j.soilbio.2009.02.007

Nakhavali, M., Friedlingstein, P., Lauerwald, R., Tang, J., Chadburn, S., Camino-Serrano, M., et al. (2018). Representation of dissolved organic carbon in the JULES land surface model (vn4.4_JULES-DOCM). *Geoscientific Model Development*, *11*(2), 593–609. https://doi.org/10.5194/gmd-11-593-2018

Nakhavali, M., Lauerwald, R., Regnier, P., Guenet, B., Chadburn, S., & Friedlingstein, P. (2020). Leaching of dissolved organic carbon from mineral soils plays a significant role in the terrestrial carbon balance. *Global Change Biology*, *27*(5), 1083–1096. https://doi.org/10.1111/gcb.15460

Nash, J., & Sutcliffe, I. (1970). River flow forecasting through conceptual models. A Discussion of Principles. *Journal of Hydrology*, *10*(3), 282–290. https://doi.org/10.1016/0022-1694(70)90255-6

Neff, J. C., & Asner, G. P. (2001). Dissolved organic carbon in terrestrial ecosystems: Synthesis and a model. *Ecosystems*, *4*(1), 29–48. https://doi.org/10.1007/s100210000058

Quinton, J. N., Govers, G., Van Oost, K., & Bardgett, R. D. (2010). The impact of agricultural soil erosion on biogeochemical cycling. *Nature Geoscience*, *3*(5), 311–314. https://doi.org/10.1038/ngeo838

Ran, L., Yang, X., Tian, M., Shi, H., Liu, S., Yu, R., & Zhou, Y. (2020). Riverine export of water, sediment and carbon during flood events in the arid to semi-arid Wuding River on the Chinese Loess Plateau. *Earth Surface Processes and Landforms*, *45*(8), 1777–1788. https://doi.org/10.1002/esp.4845

Ren, W., Tian, H., Cai, W. J., Lohrenz, S. E., Hopkinson, C. S., Huang, W. J., et al. (2016). Century-long increasing trend and variability of dissolved organic carbon export from the Mississippi River basin driven by natural and anthropogenic forcing. *Global Biogeochemical Cycles*, *30*(9), 1288–1299. https://doi.org/10.1002/2016gb005395

Silburn, D. M., & Connolly, R. D. (1995). Distributed parameter hydrology model (ANSWERS) applied to a range of catchment scales using rainfall simulator data I: Infiltration modelling and parameter measurement. *Journal of Hydrology*, *172*(1), 87–104. https://doi.org/10.1016/0022-1694(95)02740-g

Simonneaux, V., Cheggour, A., Deschamps, C., Mouillot, F., Cerdan, O., & Le Bissonnais, Y. (2015). Land use and climate change effects on soil erosion in a semi-arid mountainous watershed (High Atlas, Morocco). *Journal of Arid Environments*, *122*, 64–75. https://doi.org/10.1016/j.jaridenv.2015.06.002

Skjemstad, J. O., Spouncer, L. R., Cowie, B., & Swift, R. S. (2004). Calibration of the Rothamsted organic carbon turnover model (RothC ver. 26.3), using measurable soil organic carbon pools. *Australian Journal of Soil Research*, *42*(1), 79–88. https://doi.org/10.1071/sr03013

Song, C., Luan, J., Xu, X., Ma, M., Aurela, M., Lohila, A., et al. (2020). A microbial functional group-based CH4 model integrated into a terrestrial ecosystem model: Model structure, site-level evaluation, and sensitivity analysis. *Journal of Advances in Modeling Earth Systems*, *12*(4), e2019MS001867. https://doi.org/10.1029/2019ms001867

Sulla-Menashe, D., & Friedl, M. A. (2018). User guide to collection 6 MODIS land cover (MCD12Q1 and MCD12C1) product [Dataset]. USGS: EarthData Repository. https://doi.org/10.5067/MODIS/MCD12Q1.006

Tan, Z., Leung, L. R., Li, H. Y., & Cohen, S. (2022). Representing global soil erosion and sediment flux in Earth System Models. *Journal of Advances in Modeling Earth Systems*, *14*(1). https://doi.org/10.1029/2021ms002756

Thieme, L., Graeber, D., Hofmann, D., Bischoff, S., Schwarz, M. T., Steffen, B., et al. (2019). Dissolved organic matter characteristics of deciduous and coniferous forests with variable management: Different at the source, aligned in the soil. *Biogeosciences*, *16*(7), 1411–1432. https://doi.org/10.5194/bg-16-1411-2019

Tiefenbacher, A., Weigelhofer, G., Klik, A., Mabit, L., Santner, J., Wenzel, W., & Strauss, P. (2021). Antecedent soil moisture and rain intensity control pathways and quality of organic carbon exports from arable land. *Catena*, *202*, 105297. https://doi.org/10.1016/j.catena.2021.105297

Tobón, C., Sevink, J., & Verstraten, J. M. (2004). Litterflow chemistry and nutrient uptake from the forest floor in northwest Amazonian forest ecosystems. *Biogeochemistry*, *69*(3), 315–339. https://doi.org/10.1023/b:biog.0000031051.29323.27

Tückmantel, T., Leuschner, C., Preusser, S., Kandeler, E., Angst, G., Mueller, C. W., & Meier, I. C. (2017). Root exudation patterns in a beech forest: Dependence on soil depth, root morphology, and environment. *Soil Biology and Biochemistry*, *107*, 188–197. https://doi.org/10.1016/j.soilbio.2017.01.006

van Hees, P. A. W., Jones, D. L., Finlay, R., Godbold, D. L., & Lundstomd, U. S. (2005). The carbon we do not see—The impact of low molecular weight compounds on carbon dynamics and respiration in forest soils: A review. *Soil Biology and Biochemistry*, *37*(1), 1–13. https://doi.org/10.1016/j.soilbio.2004.06.010

Wang, Q., Zheng, H., Zhu, X., & Yu, G. (2015). Primary estimation of Chinese terrestrial carbon sequestration during 2001–2010. *Science Bulletin*, *60*(6), 577–590. https://doi.org/10.1007/s11434-015-0736-9

Wang, S., Wang, X., He, B., & Yuan, W. (2020). Relative influence of forest and cropland on fluvial transport of soil organic carbon and nitrogen in the Nen River basin, northeastern China. *Journal of Hydrology*, *582*, 124526. https://doi.org/10.1016/j.jhydrol.2019.124526

Wang, X., Quine, T. A., Zhang, H., Tian, G., & Yuan, W. (2019). Redistribution of soil organic carbon induced by soil erosion in the nine River Basins of China. *Journal of Geophysical Research: Biogeosciences*, *124*(4), 1018–1031. https://doi.org/10.1029/2018jg004781

Whipps, J. M. (1990). Carbon economy. In J. M. Lynch (Ed.), *The rhizosphere* (pp. 59–97). Wiley.

Wickland, K. P., Neff, J. C., & Aiken, G. R. (2007). Dissolved organic carbon in Alaskan boreal forest: Sources, chemical characteristics, and biodegradability. *Ecosystems*, *10*(8), 1323–1340. https://doi.org/10.1007/s10021-007-9101-4

Willey, J. D., Kieber, R. J., Eyman, M. S., & Avery, G. B. (2000). Rainwater dissolved organic carbon: Concentrations and global flux. *Global Biogeochemical Cycles*, *14*(1), 139–148. https://doi.org/10.1029/1999gb900036

Wischmeier, W., & Smith, D. (1978). Predicting rainfall erosion losses—A guide to conservation planning. *Agriculture Handbooks (USA)*, *537*, 62.

Xia, J., Liu, S., Liang, S., Chen, Y., Xu, W., & Yuan, W. (2014). Spatio-temporal patterns and climate variables controlling of biomass carbon stock of global grassland ecosystems from 1982 to 2006. *Remote Sensing*, *6*(3), 1783–1802. https://doi.org/10.3390/rs6031783

Yang, Y. D., Kanae, S., Oki, T., Koike, T., & Musiake, K. (2003). Global potential soil erosion with reference to land use and climate changes. *Hydrological Processes*, *17*(14), 2913–2928. https://doi.org/10.1002/hyp.1441

Yoo, K., Amundson, R., Heimsath, A. M., & Dietrich, W. E. (2005). Erosion of upland hillslope soil organic carbon: Coupling field measurements with a sediment transport model. *Global Biogeochemical Cycles*, *19*(3), GB3003. https://doi.org/10.1641/B570408

You, Y. Y., Xiang, W. H., Ouyang, S., Zhao, Z. H., Chen, L., Zeng, Y. L., et al. (2020). Hydrological fluxes of dissolved organic carbon and total dissolved nitrogen in subtropical forests at three restoration stages in southern China. *Journal of Hydrology*, *583*, 124–656. https://doi.org/10.1016/j.jhydrol.2020.124656

Yuan, W. P., Liu, D., Dong, W. J., Liu, S. G., Zhou, G. S., Yu, G. R., et al. (2014). Multiyear precipitation reduction strongly decreases carbon uptake over northern China. *Journal of Geophysical Research: Biogeosciences*, *119*(5), 881–896. https://doi.org/10.1002/2014jg002608

Yuan, W. P., Piao, S. L., Qin, D. H., Dong, W. J., Lin, H., & Chen, M. (2018). Influence of vegetation growth on the enhanced seasonality of atmospheric CO_2. *Global Biogeochemical Cycles*, *32*(1), 32–41. https://doi.org/10.1002/2017gb005802

Yue, Y., Ni, J., Ciais, P., Piao, S., Wang, T., Huang, M., et al. (2016). Lateral transport of soil carbon and land-atmosphere CO_2 flux induced by water erosion in China. *Proceedings of the National Academy of Sciences of the United States of America*, *113*(24), 6617–6622. https://doi.org/10.1073/pnas.1523358113

Zhang, H., Lauerwald, R., Regnier, P., Ciais, P., Yuan, W., Naipal, V., et al. (2020). Simulating erosion-induced soil and carbon delivery from uplands to rivers in a global land surface model. *Journal of Advances in Modeling Earth Systems*, *12*(11), e2020MS002121. https://doi.org/10.1029/2020MS002121

Zhang, H., Liu, S., Yuan, W., Dong, W., Xia, J., Cao, Y., & Jia, Y. (2016). Loess Plateau check dams can potentially sequester eroded soil organic carbon. *Journal of Geophysical Research: Biogeosciences*, *121*(6), 1449–1455. https://doi.org/10.1002/2016jg003348

Zhang, H., Liu, S., Yuan, W., Dong, W., Ye, A., Xie, X., et al. (2014). Inclusion of soil carbon lateral movement alters terrestrial carbon budget in China. *Scientific Reports*, *4*(1), 7247. https://doi.org/10.1038/srep07247

Zhang, S., Li, Q., Lu, Y., Zhang, X., & Liang, W. (2013). Contributions of soil biota to C sequestration varied with aggregate fractions under different tillage systems. *Soil Biology and Biochemistry*, *62*, 147–156. https://doi.org/10.1016/j.soilbio.2013.03.023